ISSN 0869-5911, Petrology, 2017, Vol. 25, No. 2, pp. 150–180. © Pleiades Publishing, Ltd., 2017.
Original Russian Text © A.A. Nosova, E.O. Dubinina, L.V. Sazonova, A.V. Kargin, N.M. Lebedeva, V.A. Khvostikov, Zh.P. Burmii, I.A. Kondrashov, V.V. Tret'yachenko, 2017, published in Petrologiya, 2017, Vol. 25, No. 2, pp. 135–167.

Geochemistry and Oxygen Isotopic Composition of Olivine in Kimberlites from the Arkhangelsk Province: Contribution of Mantle Metasomatism

A. A. Nosova[a, *], E. O. Dubinina[a], L. V. Sazonova[b], A. V. Kargin[a], N. M. Lebedeva[a], V. A. Khvostikov[c], Zh. P. Burmii[c], I. A. Kondrashov[a], and V. V. Tret'yachenko[d]

[a] *Institute of the Geology of Ore Deposits, Petrography, Mineralogy, and Geochemistry (IGEM), Russian Academy of Sciences, Moscow, 119017 Russia*

[b] *Geological Faculty, Moscow State University, Moscow, 119899 Russia*

[c] *Institute of Microelectronic Technology and Ultrahigh-Purity Materials, Russian Academy of Sciences, Chernogolovka, Moscow oblast, 142432 Russia*

[d] *ALROSA Research and Exploration Company, Arkhangelsk, 163045, Russia*

**e-mail: nosova@igem.ru*

Received May 28, 2015; in final form, February 17, 2016

Abstract—The paper presents data on the composition of olivine macrocrysts from two Devonian kimberlite pipes in the Arkhangelsk diamond province: the Grib pipe (whose kimberlite belongs to type I) and Pionerskaya pipe (whose kimberlite is of type II, i.e., orangeite). The dominant olivine macrocrysts in kimberlites from the two pipes significantly differ in geochemical and isotopic parameters. Olivine macrocrysts in kimberlite from the Grib pipe are dominated by magnesian (Mg# = 0.92–0.93), Ti-poor (Ti < 70 ppm) olivine possessing low Ti/Na (0.05–0.23), Zr/Nb (0.28–0.80), and Zn/Cu (3–20) ratios and low Li concentrations (1.2–2.0 ppm), and the oxygen isotopic composition of this olivine $\delta^{18}O = 5.64‰$ is higher than that of olivine in mantle peridotites ($\delta^{18}O = 5.18 \pm 0.28‰$). Olivine macrocrysts in kimberlite from the Pionerskaya pipe are dominated by varieties with broadly varying Mg# = 0.90–0.93, high Ti concentrations (100–300 ppm), high ratios Ti/Na (0.90–2.39), Zr/Nb (0.31–1.96), and Zn/Cu (12–56), elevated Li concentrations (1.9–3.4 ppm), and oxygen isotopic composition $\delta^{18}O = 5.34‰$ corresponding to that of olivine in mantle peridotites. The geochemical and isotopic traits of low-Ti olivine macrocrysts from the Grib pipe are interpreted as evidence that the olivine interacted with carbonate-rich melts/fluids. This conclusion is consistent with the geochemical parameters of model melt in equilibrium with the low-Ti olivine that are similar to those of deep carbonatite melts. Our calculations indicate that the variations in the $\delta^{18}O$ of the olivine relative the "mantle range" (toward both higher and lower values) can be fairly significant: from 4 to 7‰ depending on the composition of the carbonate fluid. These variations were formed at interaction with carbonate fluid, whose $\delta^{18}O$ values do not extend outside the range typical of mantle carbonates. The geochemical parameters of high-Ti olivine macrocrysts from the Grib pipe suggest that their origin was controlled by the silicate (water–silicate) component. This olivine is characterized by a zoned Ti distribution, with the configuration of this distribution between the cores of the crystals and their outer zones showing that the zoning of the cores and outer zones is independent and was produced during two episodes of reaction interaction between the olivine and melt/fluid. The younger episode (when the outer zone was formed) likely involved interaction with kimberlite melt. The transformation of the composition of the cores during the older episode may have been of metasomatic nature, as follows from the fact that the composition varies from grain to grain. The metasomatic episode most likely occurred shortly before the kimberlite melt was emplaced and was related to the partial melting of pyroxenite source material.

DOI: 10.1134/S0869591117010064

INTRODUCTION

The geochemistry and isotopic composition of olivine is a tool nowadays widely utilized to gain an insight into the genesis of both the olivine itself and its host rocks (Bussweiler et al., 2015; Cordier et al., 2015; Davis et al., 2013; Foley et al., 2013; Sobolev et al., 2009; Prelevic and Foley, 2007). The geochemistry of olivine is of paramount importance for those studying kimberlites (Bussweiler et al., 2015; Cordier et al., 2015; Sobolev et al., 2009, 2015) because the origin of this mineral in kimberlites has long been a matter of heated discussions (Bussweiler et al., 2015; Sazonova et al., 2015; and references therein).

When in kimberlite, olivine is usually found as crystals of two types (Clement, 1982; Mitchell, 1986; Kamenetsky et al., 2008): olivine I (macrocrysts,

which are large rounded crystals) and olivine II (small euhedral, often zoned crystals).

The extensive literature on the genesis of olivine in kimberlites can be summarized in the form of the following major groups of hypotheses: (1) the genesis of the two olivine types is different: olivine I is of xenogenic nature and is olivine grains borrowed from disintegrated mantle xenoliths, while olivine II is related to the kimberlite melt and is, in this sense, phenocrysts (Skinner, 1989; Skinner, Clement, 1979; Parsadanyan et al., 1996; *Arkhangelsk*..., 1999; Kopylova et al., 2009); (2) most olivine grains in kimberlites are related to the kimberlite melt, and the differences in their composition, size, and other properties reflect their crystals histories at different pressures (Mitchell, 1986; Moore, 1988, 2012), with the macrocrysts providing a "record" of the early metasomatism in relation to the kimberlite melt (Sobolev et al., 2015); and (3) large olivine grains and the cores of small euhedral olivine crystals are xenocrysts, while the outer zones of all grains crystallize from the kimberlite melt (Brett et al., 2009; Arndt et al., 2010; Kamenetsky et al., 2008).

In recent publications, the problem of kimberlite magmatism was solved using not only data on the concentrations of elements stoichiometric for olivine but also information derived from minor elements in this mineral (Sobolev et al., 2009; Pilbeam et al., 2013; Sazonova et al., 2015; Cordier et al., 2015) and trace elements (Bussweiler et al., 2015). These data suggest that olivine sources in kimberlites are variable, and kimberlite olivine can crystallize from kimberlite melts and/or be also produced by the recrystallization and metasomatism of olivine from the host rocks affected by the kimberlite melts.

The isotopic composition of kimberlite olivine deviates from the typical mantle one, $\delta^{18}O$ 5.2 ± 0.2‰ (Mattey et al., 1994), as has been demonstrated in (Zhang et al., 2000) for kimberlites at Kimberley, South Africa. Thereby the oxygen isotopic composition of olivine seems to be correlated with its chemical composition. Such isotopic deviations and correlations with chemical composition were also detected in olivine in continental and oceanic intraplate basalts (Liu et al., 2015; Eiler, 2001) and are reportedly explained in this instance by the contribution of continental crustal material. However, the variations in the oxygen isotopic composition of kimberlite olivine (as well as other minerals) were interpreted as formed under the effect of fluid (see, for example, Zhang et al., 2000; Huang et al., 2014), and this issue is so far poorly understood.

This publication continues a series of our earlier papers devoted to olivine in kimberlite peridotite xenoliths from the Arkhangelsk province (Sazonova et al., 2015; Kargin et al., 2016). Herein we report data obtained by studying the geochemistry of olivine macrocrysts from kimberlites (analyzed by EPMA and LA-ICP-MS) and the oxygen isotopic composition in these macrocrysts. For comparison, we have also studied the oxygen isotopic composition of olivine and pyroxenes from peridotite xenoliths. These data are utilized to discuss the specifics of crystallization and recrystallization of olivine and evaluate certain parameters of these processes.

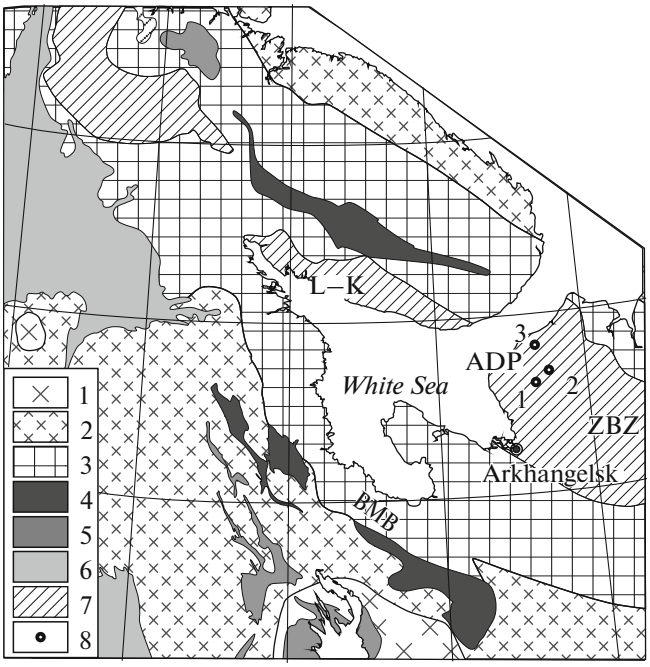

Fig. 1. Schematic map of tectonic zones in the northern East European Platform and the Arkhangelsk diamond province (ADP) on this platform (modified after Samsonov et al., 2009, 2012). (1–3) Archean crustal blocks: (1) 3.6–3.2 Ga (2) 3.0–2.7 Ga, (3) Archean crust recycled in the Paleoproterozoic; (4–7) Paleoproterozoic crustal blocks: (4) 2.5–2.3 Ga, (5) 2.30–2.05 Ga, (6) 1.95–1.75, (7) Lapland–Kola orogen, 1.98–1.85 Ga; (8) kimberlite pipes and sills (numerals in the map): 1—Pionerskaya pipe, 2—Grib pipe, 3—sills in the Mela River area. L–K is the Lapland–Kola collisional belt, ZBZ is the Zimnii Bereg zone, BMP is the Belomorian mobile belt, and ADP is the Arkhangelsk diamond province.

GEOLOGY OF THE KIMBERLITES

We have studied the composition of olivine from two economic diamond-bearing kimberlite pipes in the Devonian Arkhangelsk diamond province: the Grib and Pionerskaya pipes (Fig. 1). The *Pionerskaya pipe* in the Zolotitskoe field composes, together with the Arkhangelskaya, Karpinskaya 1, Karpinskaya 2, and Lomonosovskaya, the Lomonosov diamond deposit. The Rb–Sr age of the kimberlite is 380 ± 6 Ma (Pervov et al., 2005a). The *Grib pipe* is located in the Chernoozerskoe field, 30 km northeast of the Pionerskaya pipe. Kimberlite of the pipe has a Rb–Sr mineral isochronic age of 376 ± 3.3 Ma (Larionova et al., 2016). The geology of the pipes and their com-

position are described in much detail in numerous publications (Sablukov, 1990; Parsadanyan et al., 1996; Beard et al., 1998; *Arkhangelsk*..., 1999; Mahotkin et al., 2000; Verichev et al., 2003; Kononova et al., 2006; Bogatikov et al., 2007; Sazonova et al., 2015; and others).

The **Pionerskaya pipe** comprises two diatrems with merged craters; the thickness of the crater deposits is 150 m. The diatrems are composed of volcanic kimberlite with a variable content of xenogenic material. The gradual transition to massive macrocrystic hypabyssal rocks occurs at depths of 850–900 m (*Arkhangelsk*..., 1999; Mahotkin et al., 2000; Pervov et al., 2005a).

The **Grib pipe** possesses a preserved crater facies up to 110 m thick, which consists of units of volcaniclastic, volcanic–sedimentary, and sedimentary rocks. The diatreme zone is made up of volcaniclastic, massive pyroclastic, and hypabyssal kimberlite (Verichev et al., 2003; Kononova et al., 2007). These kimberlite varieties were recovered from depths of 600–750 m by Boreholes 106 and 1. Kimberlite in the Grib pipe contains numerous mantle peridotite and eclogite xenoliths, which were described in (Sablukov et al., 2000; Kostrovitsky et al., 2004; Golubkova et al., 2013; Shchukina et al., 2015a, 2015b; Sazonova et al., 2015; and others). Recently we obtained detailed data on a xenolith of deformed peridotite (Kargin et al., 2016) and xenoliths of mantle eclogites and garnet–clinopyroxene rocks (Nosova et al., 2015). For comparison, herein we report the oxygen isotopic composition of olivine and pyroxenes from peridotite xenoliths, which were described in (Sazonova et al., 2015).

Carbonatite–kimberlite sills were found in the Mela River area in the northern part of the Arkhangelsk diamond province, approximately 50 km north of the Grib pipe. The sills are dominated by massive hypabyssal kimberlite, including phlogopite–carbonate varieties (carbonatite) which very rarely contain olivine macrocrysts (if any) (Pervov et al., 2005b).

PETROGRAPHY

In the **Pionerskaya pipe**, olivine was studied in massive macrocrystic hypabyssal kimberlite. The material was taken from the core of Borehole 1490, which was drilled through the northwestern part of the pipe (depths 1040–1050 m, samples 13PN-1490/1042 and 13PN-1490/1050). The kimberlite consists of macrocrysts set in a groundmass (Figs. 2a, 2b). The macrocryst minerals (which account for up to 50% of the rock by volume) are olivine and more rare phlogopite. The groundmass is fine-grained and consists of abundant phlogopite (up to 45%) and grains of diopside, carbonate, olivine, serpentine, and ore minerals, which are dominated by Cr-spinel. The rock also often contains the Ca–Na silicate mineral pectolite (Sazonova et al., 2015). The macrocrysts are elongate (the aspect ratio is close to 2 : 1) or equant grains with rounded contours, ranging from 3–5 to 15–20 mm in length. The rock occasionally contains chipped fragments of such grains. Olivine is serpentinized along cracks and in outer zones.

The olivine macrocrysts show poor zoning in BSE image and sometimes also thin fragments of outer zones richer in Fe, with these zones likely mostly replaced by serpentine. The olivine sometimes hosts orthopyroxene and, more rarely, clinopyroxene inclusions. According to their color, the olivine macrocrysts are classified into two types: (1) colorless or very pale greenish and (2) obviously yellow. These two groups do not show, however, any morphological differences (Sazonova et al., 2015).

In the **Grib pipe**, the *pyroclastic kimberlite* in our sample consists of macrocrysts and pyroclasts [according to the systematics of clasts in kimberlites (Scott Smith et al., 2013), which are conventionally referred to as autoliths in ADP kimberlites], which occur in a fine-grained matrix (Figs. 2c–2e). Sample 106-607 contains no more than a few percent pyroclasts. They are rounded, fractions range from a few millimeters to a few centimeters, and consist of magmatic kimberlite and sometimes contain kernels of garnet peridotite or olivine grains, which are commonly completely serpentinized. Macrocrysts make up 30 to 50 vol % of the rock and are dominantly olivine and also phlogopite, picroilmenite, garnet, clinopyroxene, and more rare orthopyroxene. The carbonate–serpentine matrix abounds in dust of opaque minerals and contains phlogopite flakes, which sometimes form accumulations and host small barite grains. The rock of sample 13Gr1-749 contains less pyroclasts and up to 50% macrocrysts, mostly olivine. The matrix of the kimberlite is micro- to fine-grained and hosts abundant Ti-rich minerals, such as picroilmenite, rutile, perovskite (which is often replaced by titanite), and carbonate. The aggregates of secondary minerals in the matrix consist of carbonate, serpentine, and rare saponite.

The morphology of olivine crystals in kimberlite from the Grib pipe is similar to that in kimberlite from the Pionerskaya pipe, but the former more often contains irregularly shaped and angular grains and the latter is strongly dominated by rounded macrocrysts (Fig. 2). Macrocrysts in kimberlite from the Grib pipe are strongly dominated by colorless or very pale yellowish gray crystals. They are extensively serpentinized and very rarely contain preserved unaltered olivine relics.

It should be mentioned that some depth intervals of the core of Boreholes 106 and 1 do contain large olivine grains that are only partly serpentinized and contain relatively large unserpenitized olivine relics. We have sampled kimberlite from these intervals to study their olivine: these are our samples 106-607 and

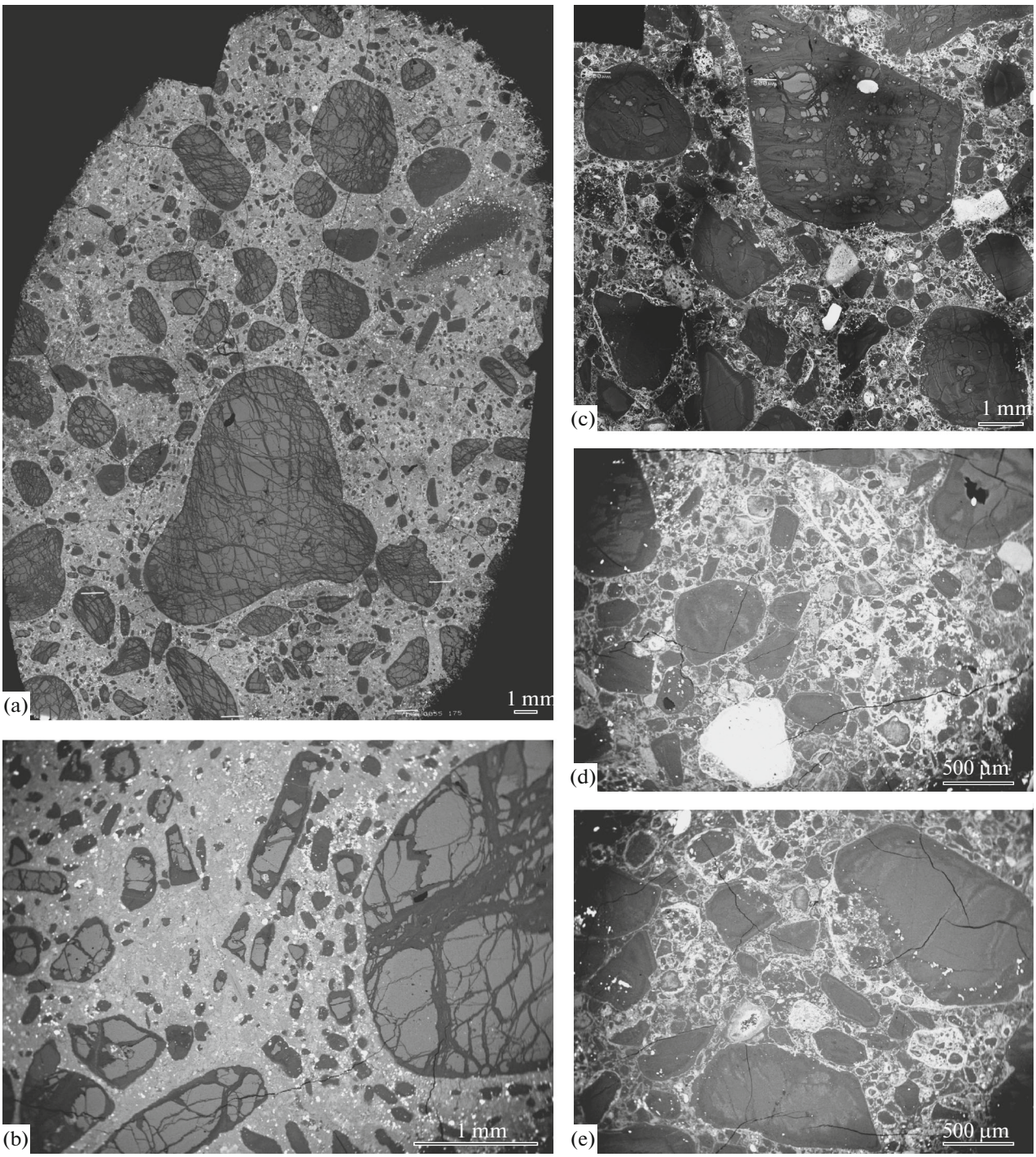

Fig. 2. Back-scattered electron images of kimberlites from (a, b) the Pionerskaya and (c, d) Grib pipes. (a, b) Massive macrocrystic hypabyssal kimberlite from the Pionerskaya pipe. The macrocrysts are olivine, the groundmass is micro- to fine-grained and consists of abundant phlogopite, grains of diopside, carbonate, pectolite, olivine, serpentine, and opaque minerals (mostly Cr-spinel). (c, e) Pyroclastic kimberlite from the Grib pipe. The rock consists of macrocrysts of extensively serpentinized olivine, with unaltered olivine preserved as relics (c), ilmenite [large white grain in the bottom part (d)] and rounded pyroclasts (autoliths) in a fine-grained matrix. The matrix consists of small olivine grains, phlogopite flakes, opaque minerals, carbonate–serpentine aggregates, and occasional barite grains.

13Gr1-749, which represent pyroclastic kimberlite with abundant macrocrysts (Figs. 2c–2d).

METHODS

The rocks were analyzed for **major components** by XRF at the Institute of the Geology of Ore Deposits, Petrography, Mineralogy, and Geochemistry (IGEM), Russian Academy of Sciences, on a PW-2400 (Philips Analytical B.V.) sequential spectrometer. Samples were prepared for analysis for major components by fusing the powdered material of the sample (0.3 g) with Li tetraborate (3 g) in an induction furnace and casting homogeneous glassy disks. The analyses were accurate to 1–5% for elements whose concentrations were higher than 0.5 wt % and 12% for elements whose concentrations were lower than 0.5 wt %.

Minor and trace elements were analyzed by ICP-MS at IGEM, with the samples preparatorily decomposed by acids. The powdered material of the sample (50–100 mg) was decomposed in Savillex Teflon vials by mixture of concentrated 1.5 mL (HF + HNO_3 in the proportion 5 : 1) and 0.5 mL HCl in a Milenstone microwave oven in fast heating mode (400 W) for 3 min and subsequent long-time (for 35 min) treating with microwave radiation (250 W). The metal fluorides were decomposed by means of triple boiling the material until dry in concentrated HCl and then pouring the material with 1 mL HCl and adding 0.5 N HNO_3 to a volume of 50 mL. If needed, additional dilution was made by the weight technique. The final concentration of HNO_3 was 0.5 N, and the dilution coefficient of the sample was 8000 to 10000 depending on the concentration of major components. Simultaneously with its final dilution, the sample was spiked with In solution (as the internal standard) in an amount needed to reach its concentration of 10 ppb in the sample.

The samples were decomposed and diluted with acids, which had been preparatorily distilled from original chemicals until a special purity grade and double diluted with distilled water.

The experiments were carried out in an X-Series II mass spectrometer with ionization in inductively coupled plasma. The material of the sample was introduced into the mass spectrometer with Ar flow as aerosol. Ions were separated by an analyzer with a double focusing system (magnetic and electrostatic). Ions were detected using an electron multiplier that preserved linearity throughout the whole range of 1 to 1×10^{10} ions per sec.

The sensitivity of the analyzer was calibrated over the mass scale using standard reference multielemental (68 elements) solutions (ICP-MS-68A, HPS, solutions A and B), which contained all elements analyzed in the samples. To control the quality of analysis and account for the drift in the sensitivity, analyses of the samples were alternated with analyses of a standard with a frequency of 1 : 10. The standards were certified samples BHVO-2 and COQ-1, which were decomposed together with the set of our samples to be analyzed. The detection limits were 0.1 ppb for elements of heavy and intermediate atomic weight and up to 1 ppb for light elements. The analyses were accurate to 1–3%. The concentrations of elements were calculated using a set of calibration solutions prepared from standard reference solution ICP-MS-68A, HPS (A and B) over a concentration range of 0.03–10 ppb.

The concentrations of **major components and elements commonly contained in olivine (Ti, Ni, Mn, Al, and Co)** were analyzed on a microprobe at the Laboratory for Analysis of Mineral Materials at IGEM, using a high-precision technique (Batanova et al., 2015) adapted at IGEM (Kargin et al., 2014; Sazonova et al., 2015). The analytical errors when studying zoned olivine crystals in kimberlite form the Pionerskaya pipe were no higher than 14–10% for Ti (2σ) at 70–100 ppm concentrations, 10–6% at 100–150 ppm, 6–5% at 150–200 ppm, and 5–4% at 200–300 ppm; 8% (2σ) for Ca, Cr, and Co at their concentrations within the analyzed ranges; and better than 1% for Mn and Ni. The error of Mg# was estimated at no worth than 0.1 mol %.

Olivine was studied in thin sections and polished pellets. To prepare the latter, a portion of each sample used to manufacture thin sections was hand-crushed, pulverized, and sieved to preserve as much as possible the size fraction –0.5 to +0.1 mm. The fraction was carefully washed and dried and then utilized to hand-pick intact olivine macrocrysts under a binocular. The grains were then poured with epoxy resin to manufacture pellets, which were then manually polished using diamond paste to expose olivine grains.

The rocks were studied on a Jeol JSM-6480LV scanning electron microscope at the Laboratory of High-Resolution Analytical Techniques at the Geological Faculty of the Moscow State University.

The concentrations of **trace elements in olivine** were analyzed by LA-ICP-MS on XSeries II (Thermo Scientific, United States) mass spectrometer equipped with a UP266 MACRO (New Wave Research, United States) system at the Institute of Microelectronic Technology and Ultrahigh-Purity Materials, Russian Academy of Sciences. We got analyzed olivine grains ranging from 0.3 to 1.5 mm, which were preparatorily examined under an electron microprobe. The energy of the laser pulse and the beam diameter were selected to ensure, on the one hand, the required sensitivity of the analysis and, on the other, to preclude the complete decomposition of the analyzed material. Each sample was analyzed at two to six spots, and the results were then averaged. The results with errors greater than 2σ were rejected. The analytical errors were up to 30%.

For external calibration with standard reference samples NIST SRM-610–SRM-616, we made use (when possible) two or more isotopes free of poly-

Table 1. Isotopes and detection limits (DL) of elements analyzed in our olivine samples ($n = 6$, $P = 0.95$)

Element	Isotope	Resolution	DL, ppm
Li	^{7}Li	0.8	0.08
B	^{10}B, ^{11}B	0.8	0.8
Na	^{23}Na	0.8	50
Mg	^{24}Mg, ^{25}Mg, ^{26}Mg	0.4	–
Al	^{27}Al	0.4	3
Si	^{29}Si	0.4	–
Ca	^{43}Ca, ^{44}Ca	0.8	50
Ti	^{47}Ti, ^{50}Ti	0.8	0.7
V	^{51}V	0.8	0.1
Cr	^{52}Cr, ^{53}Cr	0.8	1
Fe	^{54}Fe, ^{56}Fe, ^{57}Fe	0.4	–
Mn	^{55}Mn	0.8	0.3
Co	^{59}Co	0.8	0.02
Ni	^{58}Ni, ^{60}Ni	0.8	50
Cu	^{63}Cu, ^{65}Cu	0.8	0.9
Zn	^{66}Zn, ^{68}Zn	0.8	2
Zr	^{90}Zr, ^{91}Zr	0.8	0.04
Nb	^{93}Nb	0.8	0.02

atomic interferences (Table 1). When calibrating, we took into account both certified concentrations of elements in the samples and literature data on other elements that were not certified at NIST (Jochum et al., 2011). The internal standard was the ^{29}Si isotope, and the concentrations of elements were calculated by averaging over all isotopes with regard for their abundances. The correction for the possible matrix effect was carried out by normalizing the concentrations of major oxides (SiO_2, MgO, and FeO) to 100 wt %.

The detection limits of elements in olivine (Table 1) were determined by analyzing synthetic sapphire, silicon carbide, and the SRM-616 standard. The detection thresholds for most elements ranged from 1×10^{-9} to 1×10^{-7} wt %. The reason for the relatively high detection threshold of certain elements was polyatomic interferences: ^{45}Sc ($^{29}Si^{16}O$), ^{72}Ge ($^{56}Fe^{16}O$); and the high detection thresholds of Na, K, Ca, and Ni are explained by their high concentrations in both the standards and the reference samples.

The accuracy of the analyses was tested by comparing the results of LA-ICP-MS analyses with data obtained at IGEM by analyzing the same samples by a microprobe (Fig. 3). The differences for major elements (Si, Mg, and Fe) were within 2–3% on average, and the differences for Ni, Mn, Ti, Cr, and Co did not exceed 15–20% (the detection thresholds of other elements are below the detection limits of the electron microprobe).

The **oxygen isotopic composition** of olivine was analyzed by fluorination with laser heating (Sharp, 1990) at IGEM. Heating was induced by a 30W CO_2 laser in a Br penthafluoride atmosphere. Samples for an individual analysis ranged between 1 and 1.5 mg. The $^{18}O/^{16}O$ ratio of oxygen from the sample was measured on a DELTAplus (Finnigan) mass spectrometer with a double inlet system. The measurements were calibrated on the V-SMOW scale using the NBS-28 (9.58‰) and UWG-2 (5.80‰, Valley et al., 1995) internationally certified standards. In the course of the analysis, we also analyzed internationally certified reference samples: UWG-2 (garnet) and San Carlos olivine. At our calibrations, the measured $\delta^{18}O$ values of the international standard NBS-30 was 5.16‰ ($n = 8$) at recommended $\delta^{18}O = 5.10$‰, and that of San Carlos olivine was 5.25‰ ($n = 12$). According to multiple measures of international in in-house standards, the analytical error was no greater than ±0.1‰ (1σ).

RESULTS

Geochemical characteristics of our kimberlite samples are summarized in Table 2. Available geochemical data led us to classify kimberlite from the Grib pipe with kimberlites of group I, whereas kimberlite from the Pionerskaya pipe affiliate with kimberlites of group II (Fig. 4) in compliance with the systematics (Smith et al., 1985). The kimberlites of both pipes are

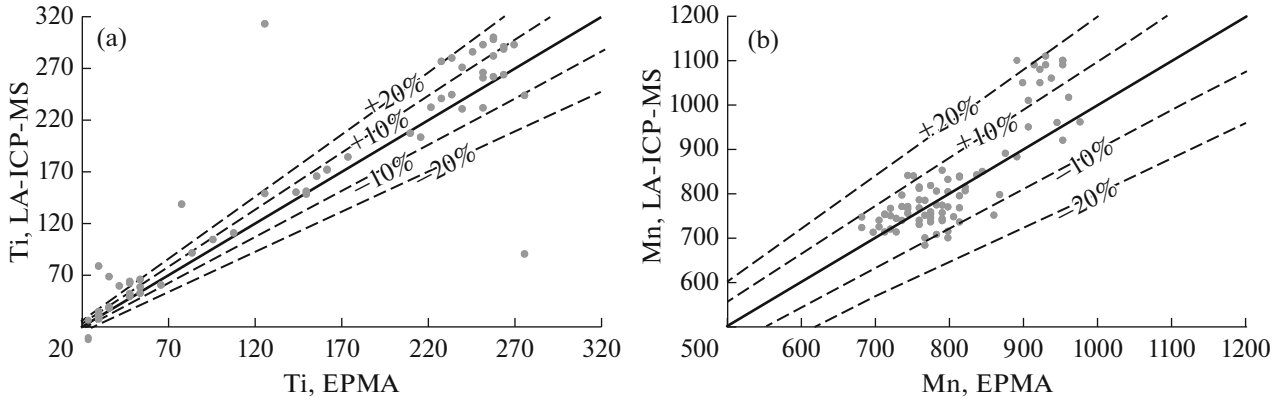

Fig. 3. Correlations between EPMA and LA-ICP-MS analyses of olivine for (a) Ti and (b) Mn.

magnesian, Mg# = 0.89, and contain closely similar concentrations of TiO_2 (≈1.0 wt %). Kimberlite from the Pionerskaya pipe is thereby richer in Mg, Fe, and Al but poorer in Si. Moreover, the latter rock is significantly enriched in K and possesses potassic alkalinity (Na_2O/K_2O = 0.04–0.2), while kimberlite from the Grib pipe contains much less K and its alkalinity is sodic (Na_2O/K_2O = 0.9–1.4). Kimberlite from the Pionerskaya pipe is richer in Rb and Ba. The primitive mantle normalized multielement patterns in Fig. 5 show the compositions of our samples and the compositions close to those of the parental melts of kimberlites of groups I and II of South Africa (Becker and Le Roex, 2006). Kimberlite from the Grib pipe is noted for a deep K anomaly, lower Ba, Rb, and Pb concentrations, and a lower Cr content (Table 2), which is a persistent difference between the kimberlites of groups I and II (Becker and Le Roex, 2006). At the same time, the Ti, Nb, and Ta concentrations of kimberlites from both pipes are similar, and the Nb and Ta concentrations are higher in kimberlite from the Pionerskaya pipe (Table 2), which does not match the relations between these elements in South African kimberlites of groups I and II (Becker and Le Roex, 2006).

The REE patterns of kimberlite from the Grib pipe are more fractionated at LREE and those of kimberlite from the Pionerskaya pipe are more fractionated at HREE: $(La/Sm)_n$ = 6.4 and 5.5–5.7; $(Gd/Yb)_n$ = 3.2 and 5.2–5.3, respectively.

Nickel concentrations are practically equal in rocks from both pipes (approximately 1500 ppm), which confirms petrographic estimates that olivine makes up about 50% of the macrocrysts (olivine is the major concentrator of this element in kimberlite).

It can be seen that both petrographic and geochemical characteristics of our kimberlite samples suggest that they are varieties of hypabyssal macrocrystic or similar type (pyroclastic but with a relatively low percentage of pyroclasts) and contain practically no xenogenic material from the host rocks. The geochemistry of kimberlite from the Grib pipe is close to that of archetypical kimberlites of group I, whereas kimberlite from the Pionerskaya pipe shows geochemical and petrographic similarities with kimberlites of group II (orangeites).

Geochemistry of olivine. The concentrations of major, minor and trace elements in the olivine are presented in Tables 3–5 and Fig. 6.

Olivine macrocrysts in kimberlite from the Pionerskaya pipe display relatively broad Mg# ranges of 0.90 to 0.93 and similar correlations between Mg# and the concentrations of such elements as Na, Mn, Zn, Cu, and V: a decrease in the Mg# of the olivine is associated with an increase in the concentrations of these elements (Fig. 6). According to the concentrations of minor elements (Ti, Ni, Cr, etc.), the olivine can be subdivided into two groups (A and B). Macrocrysts A possess high Mg# (0.91–0.93), low Ti concentrations (<70 ppm), and high Ni concentrations (2900 ppm on average). This olivine is colorless or slightly greenish. Macrocrysts B exhibit broadly varying Mg# (0.90–0.93) and high Ti concentrations (100–300 ppm) at relatively low Ni concentrations (2700 ppm). This olivine is yellow.

Macrocrysts A are richer in Ni and Cr, whereas macrocrysts B are richer in B, Li, Nb, Zr, and as was mentioned above, also in Ti (Tables 3 and 4, Fig. 6).

The concentrations of all analyzed elements in both types of the macrocrysts are as those usually found in olivine from xenoliths in kimberlites, except only for the Li and Nb concentrations, which are higher in macrocrysts B than in olivine in peridotite xenoliths and correlate with the concentrations in olivine phenocrysts (*Ol* II) in kimberlites (De Hooge et al., 2010). The Cu and Zn concentrations correspond to those usually found in large macrocrysts (*Ol* I) in kimberlites (De Hooge et al., 2010).

Table 2. Chemical composition of kimberlites from the Grib and Pionerskaya pipes

Component	Grib pipe		Pionerskaya pipe	
	13Gr1-749-1	13Gr1-759-3	13PN-1490/1042	13PN-1490/1050
SiO_2	40.23	39.08	36.06	36.64
TiO_2	1.11	1.17	1.09	0.92
Al_2O_3	1.49	1.38	3.02	2.66
Fe_2O_3	7.65	7.5	8.48	8.03
MnO	0.123	0.11	0.168	0.153
MgO	30.73	30.76	33.92	34.11
CaO	3.48	4.2	4.36	4.92
Na_2O	0.59	0.42	0.09	0.41
K_2O	0.41	0.44	2.35	2.16
P_2O_5	0.1	0.12	0.32	0.32
LOI	13.5	14.23	9.3	8.86
Total	99.413	99.41	99.158	99.183
CO_2	1.16	2.29	1.2	0.97
S	0.03	0.03	0.07	0.09
Mg#	0.89	0.89	0.89	0.89
Li	47	21	8	6
Be	1	1	3	3
Sc	5	6	11	9
V	70	70	66	89
Cr	1086	1113	1738	1630
Co	83	83	86	86
Ni	1577	1458	1426	1496
Cu	42	44	88	48
Zn	51	42	66	63
Rb	18	21	61	52
Sr	202	321	557	519
Y	5	4	8	6
Zr	46	42	90	62
Nb	38	38	59	47
Mo	0.02	<dl	0.02	<dl
Cs	0.56	0.85	1.52	0.87
Ba	185	310	786	639
La	22.0	22.0	40.6	34.2
Ce	39.3	38.4	71.5	60.6
Pr	4.3	4.2	8.4	7.0
Nd	15.3	15.0	30.8	25.5
Sm	2.2	2.2	4.8	3.9
Eu	0.6	0.6	1.3	1.0
Gd	1.4	1.4	3.0	2.4
Tb	0.21	0.19	0.42	0.35
Dy	1.09	0.98	1.93	1.57
Ho	0.17	0.15	0.29	0.24
Er	0.42	0.39	0.63	0.55
Tm	0.05	0.04	0.08	0.07
Yb	0.33	0.33	0.47	0.37
Lu	0.05	0.04	0.06	0.05
Hf	1.2	1.1	2.3	1.6
Ta	2.5	2.4	2.9	2.4
Th	3.1	3.0	4.2	3.7
U	0.7	0.6	0.8	0.7
Pb	2.6	1.6	5.6	6.4

Here and in Tables 3–6, oxides are given in wt % and elements in ppm.

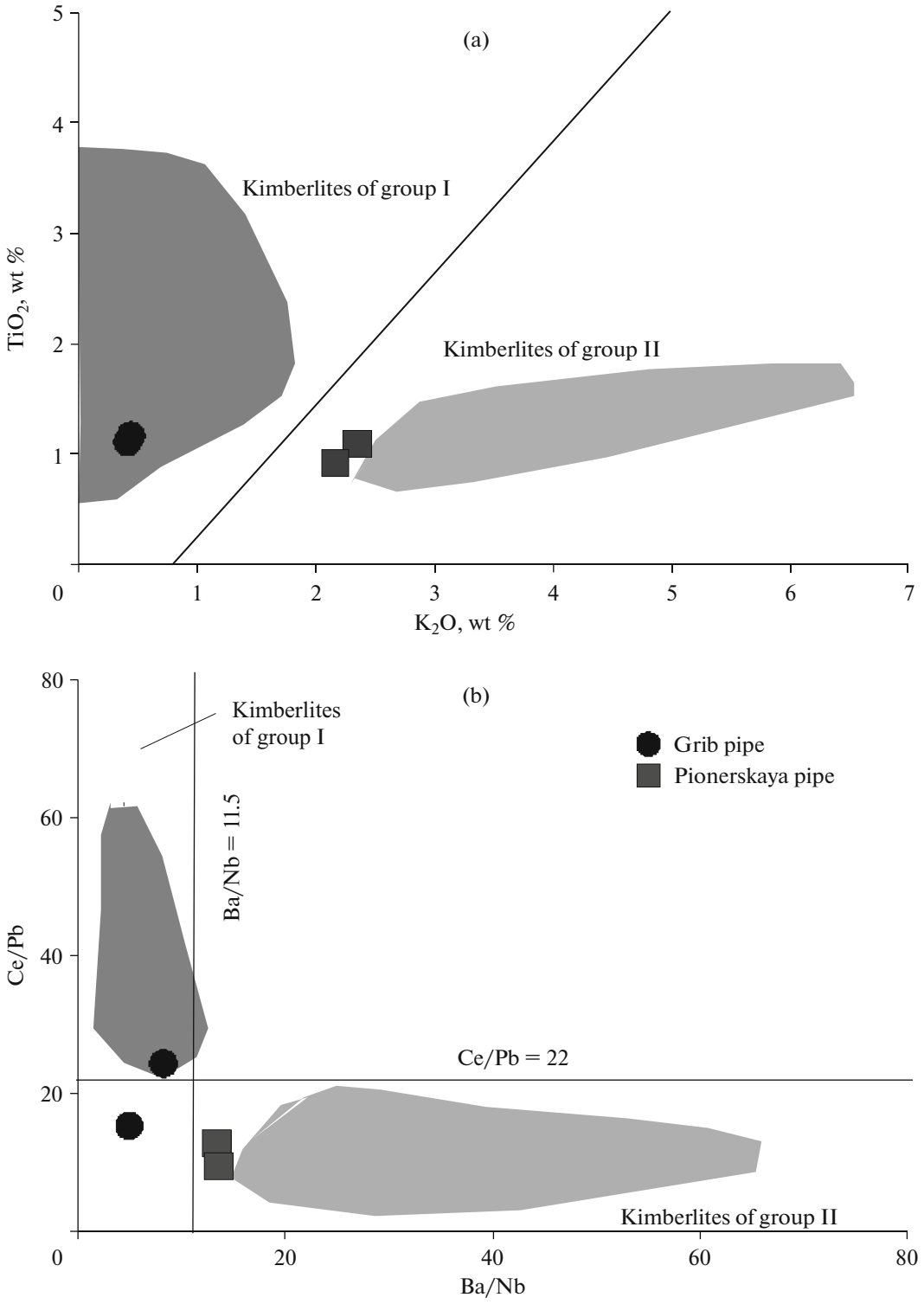

Fig. 4. (a) TiO_2–K_2O and (b) Ce/Pb–Ba/Nd diagrams for kimberlites from the Pionerskaya and Grib pipes. The composition fields and boundary lines of kimberlites of groups I and II are according to (Becker and Le Roex, 2006; Smith et al., 1985).

Olivine macrocrysts from the Pionerskaya pipe show a zonal distribution of minor elements between the cores of the grains and their outermost zones (zoning from the core to outer zone), the character of distribution of these admixtures in grain cores, and the behavior of minor elements in the outer zone (zoning in the outer zone). The compositions of macrocrysts whose zoning was examined in detail are presented in Table 6.

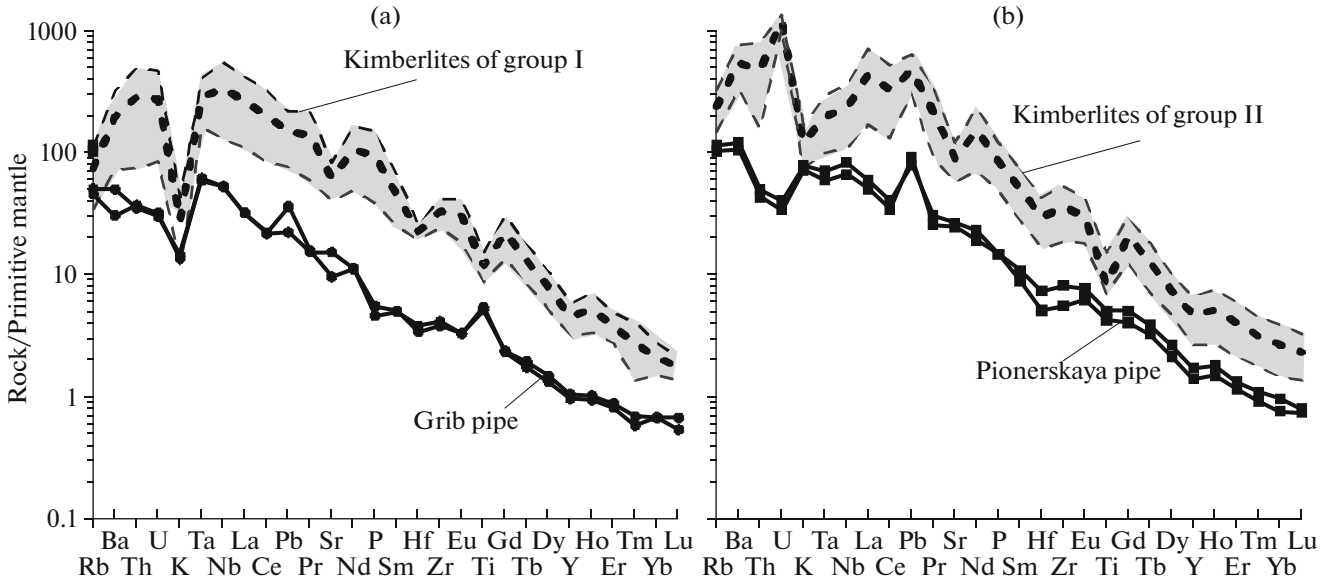

Fig. 5. Primitive mantle-normalized (Sun and McDonough, 1989) multielemental patterns of kimberlites from (a) the Pionerskaya pipe and (b) Grib pipe. Dashed lines show the compositions (± standard deviation) close to those of the partial melts of kimberlites of groups I and II in South Africa (Becker and Le Roex, 2006). Trace-element abundances are normalized to those of primitive mantle after (Sun and McDonough, 1989).

Core–outer zoning was found in the macrocrysts of both types (A and B) and is seen as a dramatic change in the concentrations of all analyzed minor elements between the cores (which are strongly dominant in crystal volumes) and thin outer zones. The BSE images of the olivine grains show obviously paler outer zones, which are richer in Fe. The outer zones are 100 to 150 μm thick. The boundaries between the outer zones and cores can be uneven and diffuse, and the material of the outer zones sometimes extends

Table 3. Composition of Ti-poor macrocrysts A hosted in kimberlite from the Pionerskaya pipe

Component	Macrocrysts A												
Mg#	0.912	0.926	0.920	0.924	0.921	0.918	0.926	0.929	0.911	0.922	0.922	0.924	0.916
SiO_2	40.79	40.99	41.09	41.19	41.16	40.96	41.16	40.77	40.93	41.39	41.47	41.47	41.30
FeO	8.53	7.21	7.74	7.39	7.70	7.93	7.21	6.78	8.59	7.60	7.56	7.34	8.10
MgO	49.36	50.32	49.95	50.51	50.02	49.65	50.13	49.66	48.97	50.20	50.02	50.09	49.53
Ti	48	24	24	18	36	30	24	84	36	54	30	30	18
Al	90	53	58	42	42	58	74	42	32	42	106	58	116
Mn	790	767	759	774	736	798	720	681	798	782	736	751	898
Ca	229	172	200	222	207	250	200	136	236	157	272	214	486
Ni	2915	3104	3080	3167	2939	3261	2947	3025	2978	3002	2263	3096	3033
Co	149	126	134	134	134	165	142	126	149	134	118	118	142
Cr	116	103	106	161	161	144	116	209	140	116	116	164	212
Li	2.9	1.4	1.7	1.8	2.0	1.9	1.8	1.8	3.9	1.9	1.9	1.9	2.0
B	–	4.5	4.1	–	4.3	4.4	4.7	4.4	–	–	–	4.3	4.8
Na	112	100	109	150	139	103	110	175	116	123	336	149	113
V	5.9	4.8	5.5	5.8	5.4	6.7	6.1	5.8	5.8	5.6	6.1	7.0	5.9
Cu	5.3	3.7	3.7	4.8	4.8	2.7	1.4	1.9	3.6	2.3	7.5	4.0	4.3
Zn	44	37	41	48	49	55	49	48	68	48	50	48	44
Zr	–	–	–	–	–	–	–	0.22	–	–	–	–	–
Nb	0.15	0.01	0.05	0.02	0.10	0.10	0.15	0.44	0.01	0.29	0.07	0.06	0.02

Here and in Tables 4 and 5, Ti, Al, Mn, Ca, Ni, Co, and Cr were analyzed by EPMA, other elements were analyzed by LA-ICP-MS; dashes mean concentrations below the detection limits.

Table 4. Composition of Ti-rich macrocrysts B hosted in kimberlite from the Pionerskaya pipe

Component	Macrocrysts B																		
Mg#	0.922	0.923	0.917	0.925	0.931	0.921	0.924	0.915	0.923	0.923	0.924	0.914	0.898	0.912	0.928	0.922	0.927	0.909	0.917
SiO_2	40.95	41.09	41.00	41.15	41.09	40.98	41.00	40.92	41.20	41.18	41.31	41.37	41.05	41.31	41.48	41.55	41.43	41.31	40.87
FeO	7.58	7.50	8.02	7.32	6.64	7.65	7.37	8.15	7.46	7.50	7.35	8.35	9.83	8.46	6.94	7.60	7.11	8.81	8.05
MgO	49.87	50.20	49.68	50.30	50.47	49.70	49.91	49.13	49.81	50.07	50.34	49.67	48.64	49.41	50.41	50.26	50.38	49.33	50.00
Ti	228	126	240	228	162	96	108	234	156	150	150	270	264	222	174	144	210	216	162
Al	48	42	21	42	21	32	37	42	37	42	42	37	48	74	32	42	42	32	42
Mn	743	736	821	821	681	767	743	875	844	767	743	836	891	813	705	720	705	960	976
Ca	179	129	121	114	121	114	143	121	114	157	114	172	179	236	121	114	107	150	114
Ni	2735	3120	2609	2907	2852	2986	2460	2593	2868	2868	2821	2907	2350	2570	2742	2962	2695	2821	2821
Co	118	142	118	134	142	149	126	126	142	142	165	173	142	157	126	134	126	157	149
Cr	92	75	123	116	113	99	171	89	147	151	137	109	72	140	99	106	106	89	72
Li	2.3	2.1	2.4	3.3	1.6	2.1	2.1	2.3	3.0	3.4	1.8	2.9	2.5	2.4	1.9	2.9	2.3	2.6	2.5
B	7.2	4.1	4.8	5.2	5.2	5.8	5.4	4.5	4.2	5.0	5.6	4.9	4.0	4.1		4.3	5.1	4.4	5.3
Na	142	128	125	147	118	107	166	123	120	146	118	162	151	170	122	112	88	103	162
V	5.3	6.1	4.8	4.2	4.9	5.3	5.4	4.5	4.0	5.3	4.9	8.5	8.8	7.5	4.6	5.0	3.5	3.8	4.0
Cu	2.5	1.4	1.5	3.4	1.1	2.3	1.1	2.3	1.4	3.5	2.3	4.6	4.3	3.8	1.7	1.2	0.8	1.3	4.7
Zn	57	45	50	46	43	47	51	61	50	51	47	55	62	54	44	50	47	61	58
Zr	0.20	0.31	0.24	0.28	0.22	0.25	0.16	0.22	0.29	0.20	0.37	–	0.18	–	0.26	0.29	0.34	0.20	0.36
Nb	0.16	0.26	0.27	0.14	0.28	1.01	0.26	0.26	0.46	0.12	0.42	0.08	0.10	0.10	0.21	0.58	0.67	0.39	1.16

Table 5. Composition of olivine macrocrysts hosted in kimberlite from the Grib pipe

Component	Macrocrysts													
Mg#	0.926	0.926	0.926	0.921	0.925	0.930	0.921	0.925	0.927	0.925	0.929	0.922	0.925	0.925
SiO_2	40.29	40.02	40.65	40.74	40.56	40.40	39.95	39.83	39.92	40.04	41.30	41.43	40.21	40.49
FeO	7.28	7.32	7.25	7.82	7.43	6.95	7.80	7.40	7.25	7.38	6.99	7.55	7.26	7.33
MgO	50.66	50.90	51.14	50.79	51.25	51.47	51.01	51.08	51.27	51.00	51.26	50.13	50.40	50.53
Ti	–	–	30	54	–	48	66	12	30	–	42	15	15	18
Al	32	21	32	48	26	32	53	26	32	26	32	42	26	42
Mn	751	774	743	798	860	712	782	790	813	774	728	774	782	759
Ca	107	107	136	207	114	100	186	114	121	100	114	179	93	107
Ni	3033	2986	3025	3033	3104	3072	3025	3065	3010	3041	3049	2947	3017	2986
Co	126	134	149	142	142	110	149	142	142	134	126	134	126	126
Cr	133	137	151	96	147	137	99	130	185	120	127	106	140	130
Li	1.30	1.70	1.40	1.90	1.40	1.50	1.60	1.20	1.40	1.40	1.32	1.80	1.60	2.00
B	5.00	4.00	5.00	6.00	4.00	10.00	4.00	3.00	4.00	3.00	1.93	4.33	3.00	6.00
Na	170	220	310	270	200	280	280	240	240	150	214	82	190	250
V	5.19	4.85	5.40	6.08	5.18	4.61	5.89	4.86	5.41	5.06	5.39	2.87	5.52	5.30
Cu	4.45	5.27	4.91	7.25	5.07	8.24	9.70	7.46	8.15	15.13	3.69	2.36	6.07	8.18
Zn	47	53	60	54	56	48	54	47	46	51	58	48	49	50
Sr	1.04	0.37	0.17	0.81	0.10	2.11	0.57	0.26	0.91	0.17	–	–	0.40	0.92
Zr	0.32	0.36	0.51	0.39		0.44	0.35	0.55	0.61	0.23	0.25		0.30	0.53
Nb	1.17	0.65	0.64	0.07	0.80	0.64	0.05	0.88	0.67	0.82	0.62	0.01	0.97	0.86
Ba	–	1.59	0.29	0.11	0.81	0.50	1.61	1.46	0.39	0.69	0.23	–	–	0.49

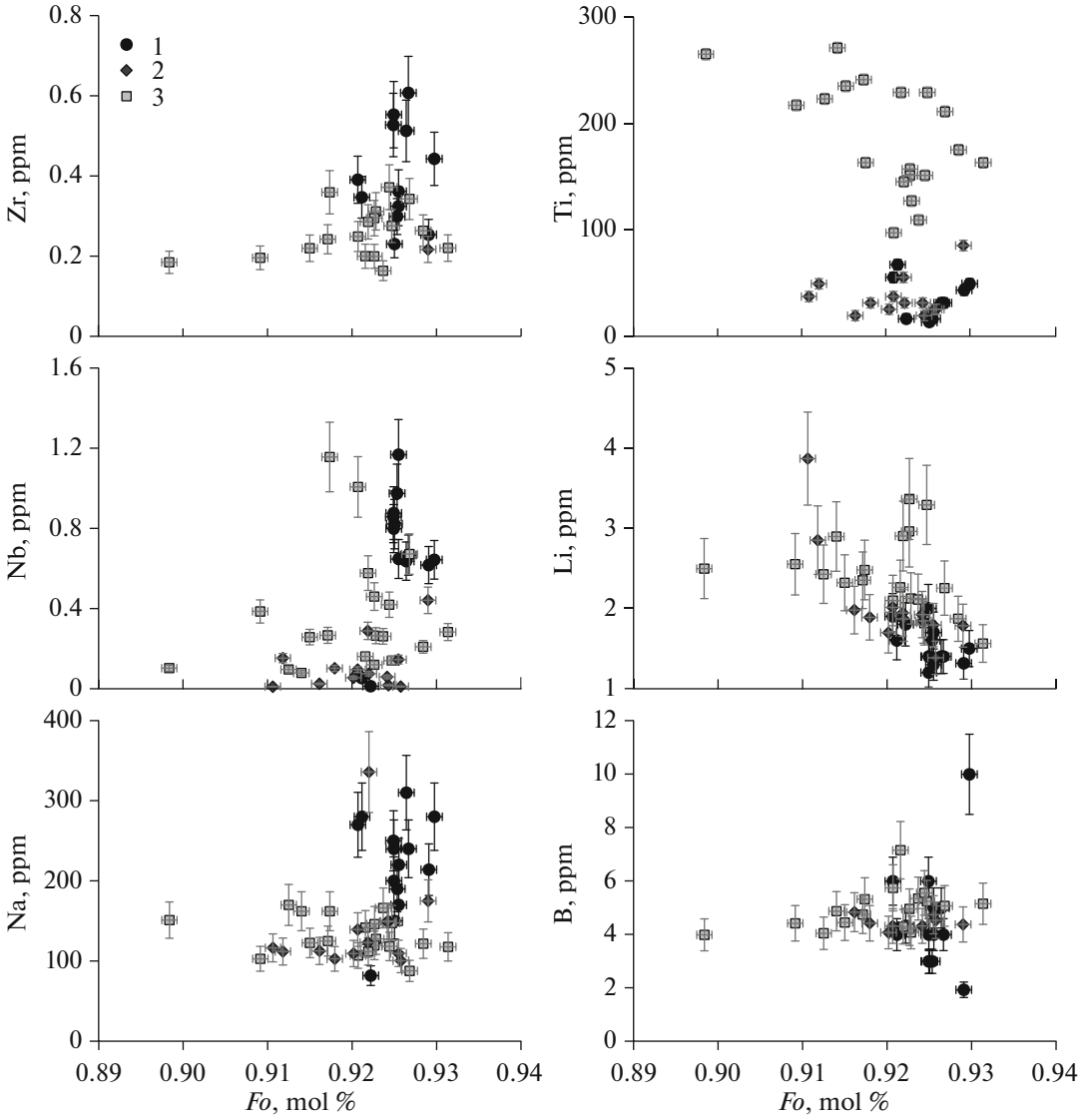

Fig. 6. Element–*Fo* diagrams for olivine macrocrysts. Olivine: (1) from the Grib pipe; (2–3) from the Pionerskaya pipe: (2) macrocrysts B, (3) macrocrysts A.

inward the olivine crystals along cracks. Large olivine grains usually preserve merely fragments of their outer zones (Fig. 7).

The outer zones of macrocrysts A possess much lower Mg# and Ni concentrations than the cores but are richer in Ti, Ca, Al, Cr, and Mn (Figs. 7d–7e, Fig. 14a). The outer zones of the macrocrysts B are also lower in Mg# and usually also Ni than the cores and are richer in Ca, Al, Cr, and Mn. The Ti distribution depends on its concentration in the core: if this concentration is no higher than 200 ppm, the Ti concentration in the outer zone increases (to 250–270 ppm), and if the concentration in the core is higher than 200 ppm, the Ti concentration in the outer decreases zone to 150 ppm (Figs. 7a–7c, Fig. 14b)

The zoning of the macrocryst cores is rarely discussed in the literature because the variations in the concentrations normally do not exceed the analytical errors. The macrocrysts of both types, A and B, usually display no zoning in Ti distribution without obvious enrichment or depletion in the outer portions of the crystal cores. However, macrocrysts B rarely show an U-shaped Ti distribution with enrichment in the outer cores (above the analytical errors) (Fig. 14c). Other elements are commonly evenly distributed in the cores (Fig. 7).

In the outer zones, Mg# decreases toward the outer boundaries of these zones, and the Al, Ti, Mn, and Ca concentrations usually increase. The distribution of Cr and Ni in the outer zones displays more complicated

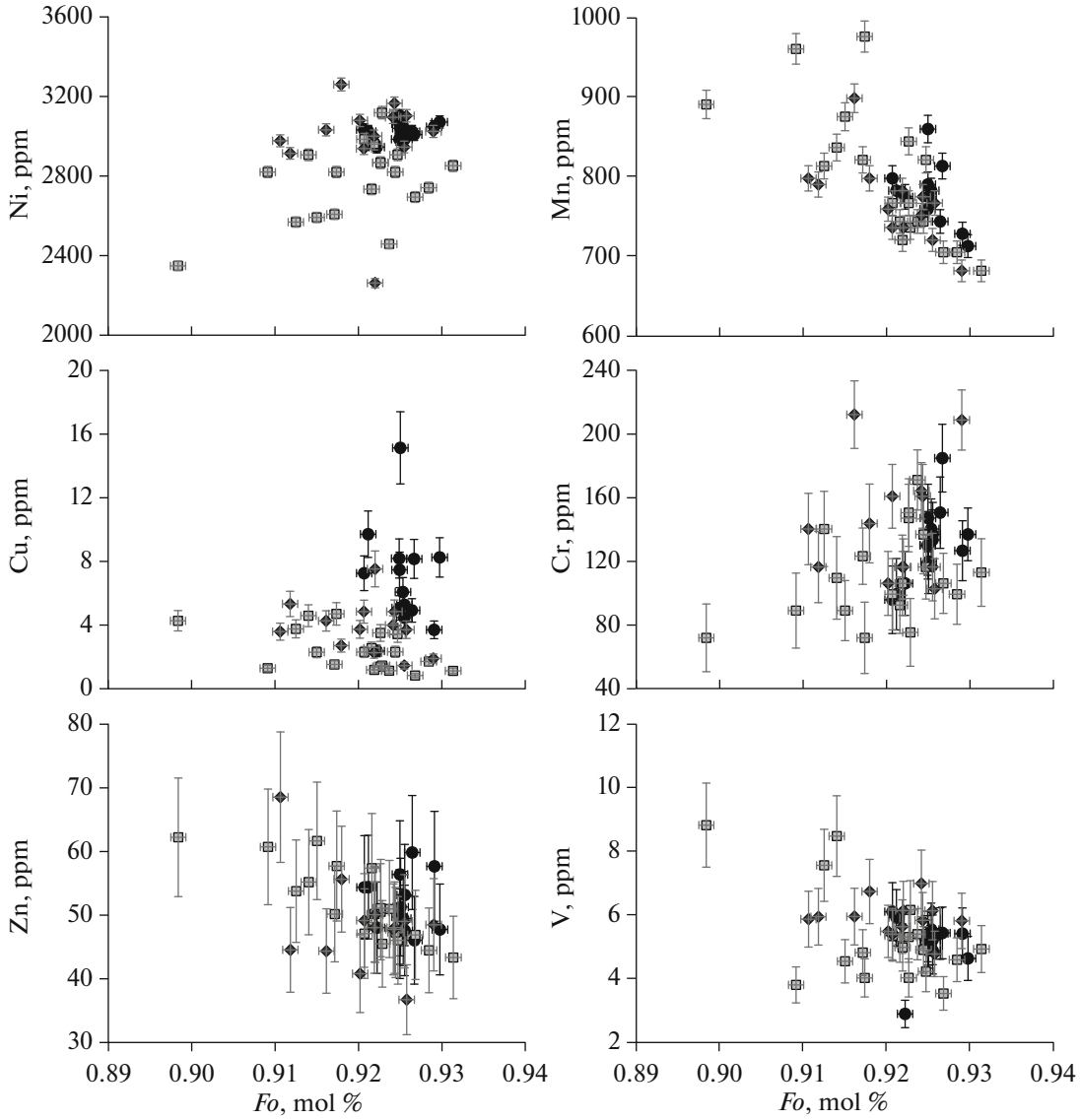

Fig. 6. (Contd.)

patterns: they increase near the inner boundaries of the outer zones and then decrease (Fig. 7e).

Olivine macrocrysts in kimberlite from the Grib pipe are noted for higher Mg# (0.92–0.93), low Ti concentrations (no higher than 70 ppm), high Ni concentrations (approximately 3000 ppm), and intermediate Cr concentrations (close to 130 ppm). They are typically rich in Nb and Zr at a variable, up to high values, Nb/Zr ratio (from 0.2 to 3.6, 1.7 on average) and relatively high Na concentrations. The Li concentrations are at a minimum in all examined macrocrysts (Table 5, Fig. 6). The level of the concentrations of certain elements (Mn, Nb, and Ti) in the olivine is more similar to those in phenocrysts (*Ol* II) than in olivine from xenoliths, and the Cu and Zr concentrations (Fig. 9) are higher than is typical of olivine in xenoliths, as described in (De Hooge et al., 2010).

The Zn/Cu and Nb/Zr ratios of the olivine significantly vary. Olivine from the Pionerskaya pipe is lower in Cu and Zr, similar to macrocrysts of types A and B, than olivine from the Grib pipe, and thereby the Zn/Cu ratio of the olivine is at the maximum and reaches 15 and 28 for macrocrysts of types A and B, respectively. Olivine from the Grib pipe is noted for enrichment in Cu at relatively low Zn concentrations and, correspondingly, low Zn/Cu ratios (9.6 on average) (Fig. 8a).

The macrocrysts of type B from the Pionerskaya pipe bear Nb concentrations similar to, and Zr concentrations lower than, Zr concentrations in olivine hosted in kimberlite from the Grib pipe, and hence, this olivine possesses higher Nb/Zr ratios (1.3 on average) (Fig. 8b). The A-type macrocrysts are depleted in these elements.

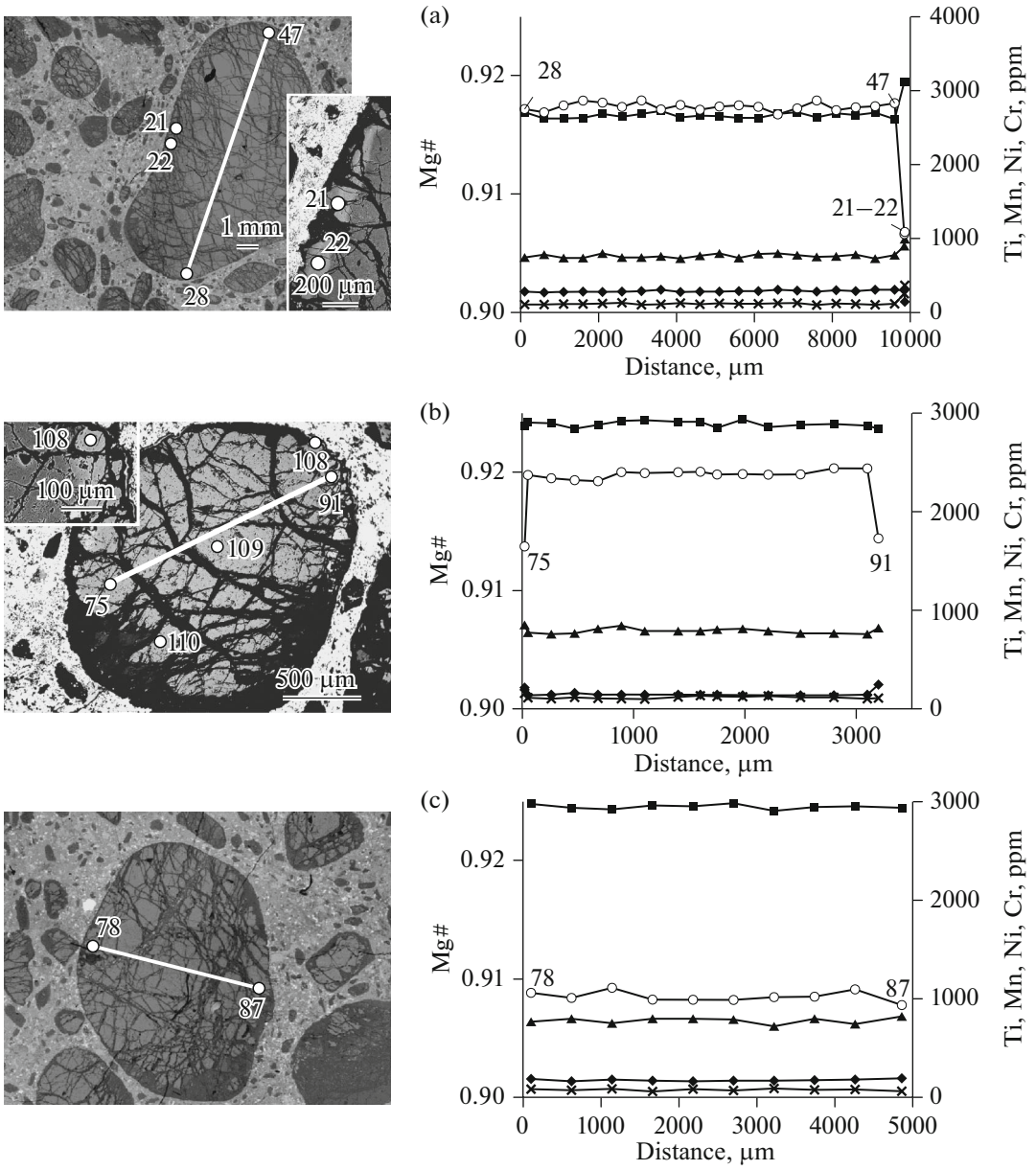

Fig. 7. Zoning in olivine macrocrysts hosted in kimberlite from the Pionerskaya pipe. (a) Large Ti-rich and high-Mg# macrocryst B (grain 1) with preserved fragments of the outermost zone (enlarged in the inset), in which Mg# and Ti concentration decrease and Ni, Mn, and Cr increase compared to those in the crystal core; (b) mildly Ti, high-Mg# macrocryst B of rounded morphology (grain 5) with a well preserved outermost zone (enlarged in the inset), in which Mg# and the Ni concentration decrease and Ti, Mn, and Cr concentrations increase compared to those in the crystal core; (c) large Ti-rich mildly Mg# macrocryst B of rounded shape (grain 2), whose outer zone is not preserved; the grain displays perceptible variations in Mg# and concentrations of elements along cracks filled with fine-crystalline aggregates of Cr-spinel, phlogopite, serpentine (pale stripe in the left-hand side); (d) fragment of a Ti-poor high Mg# macrocryst A of rounded shape (grain 12), in whose outer zone (enlarged in the inset) Mg# and Ni concentrations decrease and Ti, Mn, and Cr concentrations increase compared to those in the core; (e) low-Ti high-Mg# macrocryst A (grain 41) with rounded core and outermost zone with partially preserved crystalline habit; the boundary between the core and the outermost zone is diffuse; in the outermost zone, elements show complex behavior, but in general, Mg# and Ni concentrations decrease, while Ti, Mn, and Cr concentrations increase compared to those in the core; (f) Ti-poor mildly Mg# macrocryst A of angular–rounded morphology (grain 16), in whose outer zone (enlarged in the inset) Mg# and Ni and Mn concentrations decrease and Ti and Cr concentrations increase compared to those in the core. The analytical errors are smaller than the symbol sizes. See Table 6 for analyses of the grains (except analysis 41). Numerals in the plots correspond to the numbers of analytical spots in the BSE image.

Oxygen isotopic composition of olivine. Oxygen isotopic composition was analyzed in olivine (macrocrysts A and B) from kimberlite from the Grib and Pionerskaya pipes and, for comparison with mantle olivine in ADP, in olivine and pyroxenes from xenoliths of garnet harzburgite and garnet lherzolite hosted

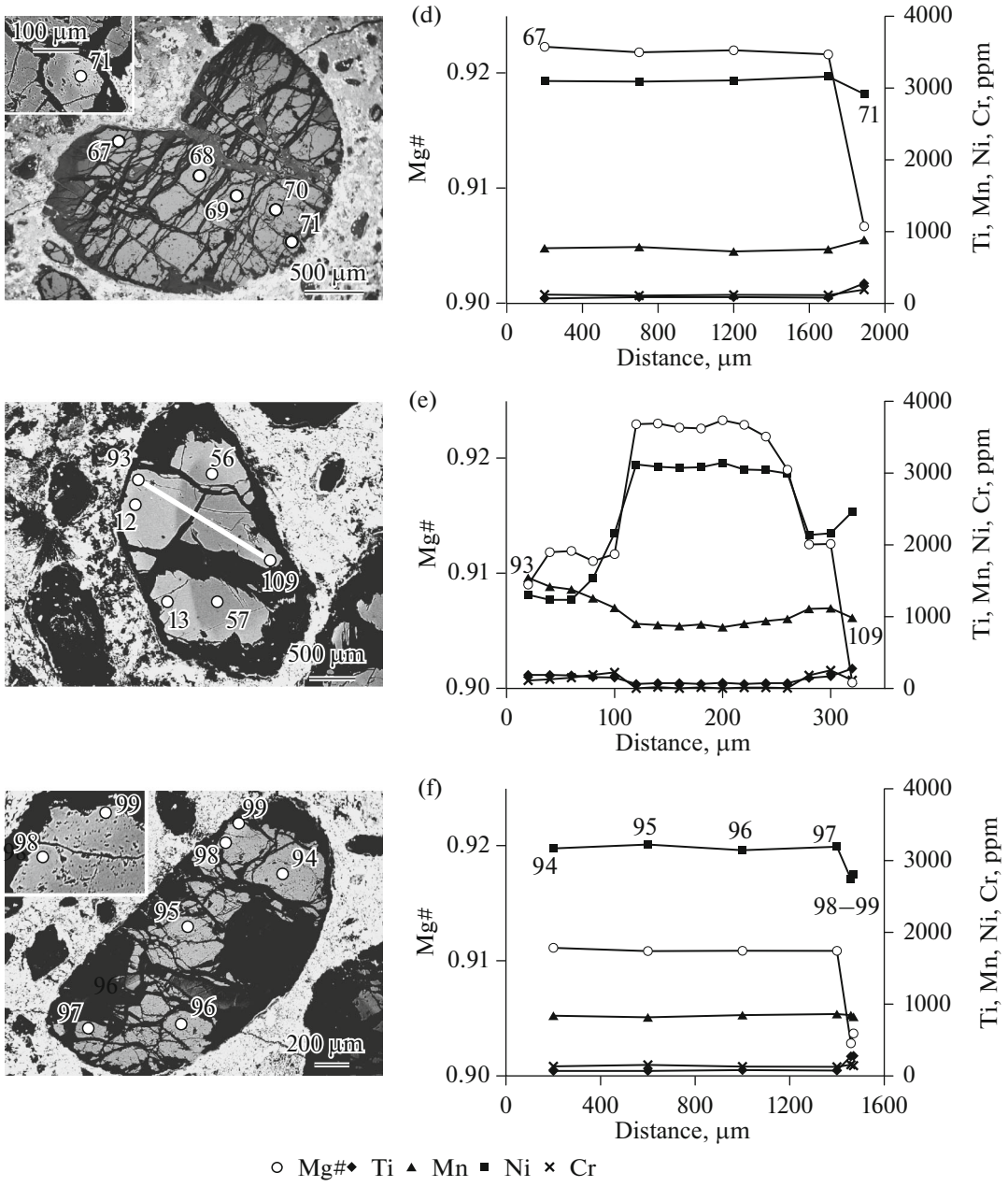

Fig. 7. (Contd.)

in kimberlite in the Grib pipe. The results are summarized in Table 7.

All olivine samples yielded $\delta^{18}O$ within the range of 5.09–5.64‰, which slightly extends outside the range of values typical of mantle olivine: 5.5 ± 0.2 (Mattey et al., 1994). The greatest $\delta^{18}O$ values were determined for olivine in kimberlite from the Grib pipe. Olivine in kimberlite from the Pionerskaya pipe show intermediate $\delta^{18}O$ values. The oxygen isotopic composition of olivine and orthopyroxene from peridotite xenoliths does not differ (within the analytical error) from the "mantle" value $\delta^{18}O$ = 5.5‰ (Table 6).

DISCUSSION

Carbonate Component in (Proto)kimberlite Melts/Fluids

Ti and Nb/Zr ratio of olivine and the role of the carbonate component. Olivine in kimberlite samples from the Grib and Pionerskaya pipes differ in both the levels of their Nb and Zr concentrations and the Zr/Nb ratio (Figs. 6, 8b). The highest Nb and Zr concentrations were found in olivine in kimberlite from the Grib pipe. Macrocrysts A from the Pionerskaya pipe possess very low Zr concentrations (Table 2). Macrocrysts B in kimberlite from the Pionerskaya pipe containing high

Table 6. Composition of zoned olivine macrocrysts hosted in kimberlite from the Pionerskaya pipe

	Macrocrysts B																					
Component	1*	1	1	1	1	1	1	1	1	1	1	1	1	1	1	1	1	1	1	1	1	1
	100**	600	1100	1600	2100	2600	3100	3600	4100	4600	5100	5600	6100	6600	7100	7600	8100	8600	9100	9600	9850	9860
	28***	29	30	31	32	33	34	35	36	37	38	39	40	41	42	43	44	45	46	47	21	22
SiO_2	41.22	41.18	41.18	41.45	41.47	41.54	41.30	41.37	41.36	41.47	41.47	41.40	41.44	41.06	41.47	41.47	41.32	41.42	41.39	41.39	41.59	41.78
Al_2O_3	0.01	0.01	0.01	0.01	0.01	0.01	0.01	0.01	0.01	0.01	0.00	0.01	0.01	0.01	0.01	0.01	0.01	0.01	0.01	0.01	0.02	0.02
FeO	8.09	8.12	8.04	8.09	8.09	8.15	8.04	8.12	8.08	8.13	8.10	8.08	8.09	8.14	8.12	8.07	8.13	8.13	8.11	8.11	9.16	9.16
MgO	50.17	50.17	50.04	50.63	50.53	50.66	50.35	50.33	50.33	50.39	50.37	50.31	50.29	50.16	50.40	50.53	50.33	50.50	50.47	50.59	49.81	49.91
CaO	0.02	0.02	0.02	0.02	0.02	0.02	0.02	0.02	0.02	0.02	0.02	0.02	0.02	0.02	0.02	0.02	0.02	0.02	0.02	0.02	0.04	0.06
CoO	0.02	0.02	0.02	0.02	0.02	0.02	0.02	0.02	0.02	0.02	0.02	0.02	0.02	0.01	0.01	0.02	0.02	0.02	0.02	0.02	0.02	0.02
Ti	282	270	276	282	276	282	288	306	276	282	282	288	288	306	294	282	300	288	306	306	300	144
Mn	743	782	736	736	798	743	743	759	728	767	798	736	790	798	774	751	759	782	728	774	898	991
Ni	2711	2625	2625	2632	2687	2648	2687	2727	2640	2664	2656	2632	2632	2687	2711	2640	2695	2672	2703	2617	3120	3120
Cr	106	106	113	113	120	130	103	109	127	109	123	116	116	123	127	99	120	113	103	116	253	366
Mg#	0.92	0.92	0.92	0.92	0.92	0.92	0.92	0.92	0.92	0.92	0.92	0.92	0.92	0.92	0.92	0.92	0.92	0.92	0.92	0.92	0.91	0.91
	Macrocrysts B																					
Component	3	3	3	3	3	3	3	2	2	2	2	2	2	2	2	2	2	10	10	10	10	10
	4450	4300	4200	3100	2200	1200	200	100	620	1140	1660	2180	2700	3220	3740	4260	4860	200	400	900	1400	2100
	72	78	73	74	75	76	77	78	79	80	81	82	83	84	85	86	87	38	39	41	40	42
SiO_2	41.08	41.31	41.08	41.34	41.42	41.39	41.47	40.89	41.24	41.02	40.64	40.74	40.70	40.50	40.86	40.85	40.38	40.97	41.10	41.24	41.16	41.04
Al_2O_3	0.01	0.00	0.01	0.00	0.01	0.01	0.00	0.01	0.01	0.01	0.01	0.01	0.01	0.01	0.01	0.01	0.01	0.01	0.01	0.01	0.00	0.01
FeO	8.55	8.77	8.71	8.76	8.76	8.73	8.72	8.92	8.91	8.88	8.90	8.93	8.92	8.79	8.89	8.83	8.83	7.75	7.85	7.85	7.86	7.81
MgO	49.72	50.14	50.00	50.08	50.09	50.09	50.08	49.76	49.46	49.80	49.32	49.50	49.41	48.86	49.40	49.47	48.68	49.74	50.13	50.18	50.12	50.01
CaO	0.07	0.02	0.02	0.02	0.03	0.02	0.02	0.03	0.03	0.03	0.03	0.03	0.03	0.03	0.03	0.03	0.06	0.02	0.02	0.02	0.02	0.02
CoO	0.01	0.02	0.01	0.02	0.02	0.02	0.02	0.02	0.02	0.02	0.01	0.02	0.02	0.02	0.02	0.02	0.02	0.02	0.02	0.02	0.02	0.02
Ti	162	264	252	264	270	270	258	186	162	180	168	162	168	168	174	180	192	162	150	150	168	174
Mn	1464	914	968	906	945	953	945	767	798	751	798	798	790	720	798	743	821	790	767	774	798	821
Ni	1242	2428	2460	2499	2483	2460	2467	2978	2939	2923	2962	2955	2986	2907	2947	2955	2939	3033	3080	3017	3080	3104
Cr	137	75	89	68	86	99	96	82	72	86	58	82	68	89	75	79	62	123	133	137	144	116
Mg#	0.91	0.91	0.91	0.91	0.91	0.91	0.91	0.91	0.91	0.91	0.91	0.91	0.91	0.91	0.91	0.91	0.91	0.92	0.92	0.92	0.92	0.92
	Macrocrysts B											Macrocrysts A										
Component	5	5	5	5	5	5	5	5	5	5	5	12	12	12	12	12	16	16	16	16	16	16
	20	50	680	890	1400	1600	2210	2500	2800	3100	3200	200	700	1200	1700	1890	200	600	1000	1400	1460	1470
	75	76	79	80	82	83	87	88	89	90	91	67	68	69	70	71	94	95	96	97	98	99
SiO_2	41.15	41.44	41.55	41.62	41.49	41.59	41.69	41.71	41.62	41.35	41.62	41.77	41.74	41.49	41.64	41.05	41.09	41.08	41.23	41.24	40.95	41.06
Al_2O_3	0.02	0.01	0.01	0.01	0.01	0.01	0.01	0.01	0.01	0.01	0.01	0.01	0.01	0.01	0.01	0.01	0.01	0.01	0.01	0.01	0.01	0.02
FeO	8.40	7.82	7.90	7.84	7.85	7.84	7.91	7.85	7.85	7.85	8.44	7.64	7.71	7.67	7.71	9.11	8.68	8.68	8.69	8.69	9.48	9.43
MgO	49.81	50.22	50.32	50.50	50.57	50.54	50.80	50.41	50.79	50.78	50.46	50.81	50.88	50.77	50.75	49.55	49.81	49.62	49.75	49.72	49.29	49.55
CaO	0.03	0.03	0.03	0.03	0.03	0.03	0.03	0.03	0.02	0.03	0.04	0.03	0.03	0.02	0.02	0.04	0.04	0.04	0.04	0.04	0.04	0.05
CoO	0.02	0.02	0.02	0.02	0.02	0.02	0.02	0.02	0.02	0.02	0.02	0.02	0.02	0.02	0.02	0.02	0.02	0.02	0.02	0.02	0.02	0.02
Ti	215	137	143	143	143	143	137	137	137	143	245	66	84	84	78	276	66	66	78	72	270	276
Mn	852	774	813	844	790	790	790	767	767	759	821	767	782	720	751	883	836	813	844	860	844	821
Ni	2868	2907	2884	2923	2915	2915	2860	2884	2892	2876	2845	3096	3088	3104	3159	2915	3167	3222	3143	3190	2742	2805
Cr	157	113	106	103	120	133	130	116	116	103	109	120	106	116	113	188	130	151	127	123	154	140
Mg#	0.91	0.92	0.92	0.92	0.92	0.92	0.92	0.92	0.92	0.92	0.91	0.92	0.92	0.92	0.92	0.91	0.91	0.91	0.91	0.91	0.90	0.90

* Grain number; ** distance from the edge of the grain, μm; *** analytical spot. Mg# = Mg/(Mg + Fe) in moles.

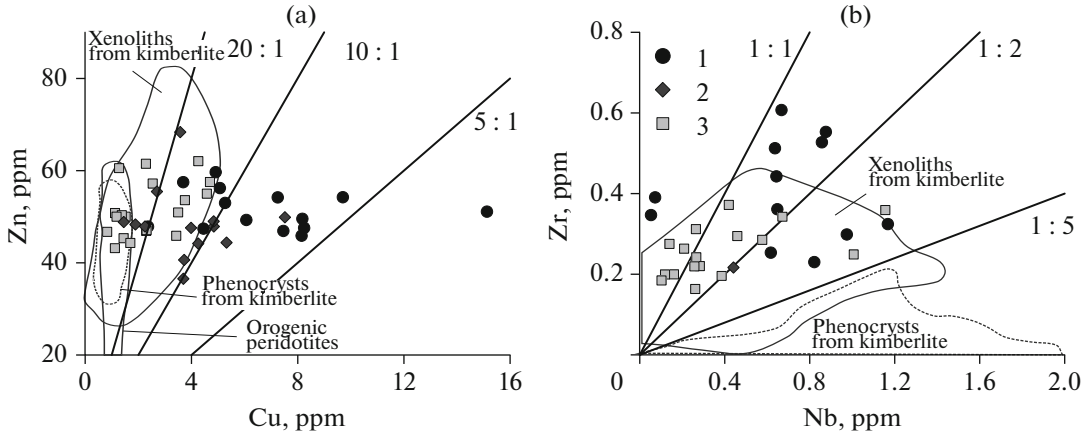

Fig. 8. (a) Zn–Cu and (b) Zr–Nb diagrams for olivine from kimberlites. Olivine: (1) from the Grib pipe; (2–3) from the Pionerskaya pipe: (2) macrocrysts B, (3) macrocrysts A. The compositional fields of olivine xenoliths and phenocrysts in kimberlites are according to (De Hooge et al., 2010).

Ti concentrations are usually noted for higher Zr/Nb ratios than those in the low-Ti olivine in kimberlite from the Grib pipe (Fig. 8b).

The incorporation mechanisms of four- and five-charged HFSE in olivine is still uncertain, even more so for the latter type. In this context, the accommodation of Ti is understood better than other elements because Ti occurrence in olivine makes this mineral able to accommodate water via the coupled substitutions

$$Mg^{2+} + Si^{4+} \rightarrow Ti^{4+} + 2H^{+},$$

which is believed to explain the dominant mechanism of water incorporation in olivine under upper mantle parameters (Schmädicke et al., 2013). The substitution of octahedral coordinated Mg for Ti can proceed via forming planar or point defects of the Ti-clinohumite type $Mg[6]TiO_2(OH)_2$ at nonzero H_2O activity (Berry et al., 2007; Shen et al., 2014). Titanium can be incorporated on both the tetrahedral T site, which is larger in olivine and is more strongly distorted than in other rock-forming minerals, and on the octahedral M site ($Mg[6]_{1.5}Ti_{0.5}AlO_4$). Other HFSE can likely occupy octahedral M sites, and the charge balance can be preserved if simultaneously mono- and/or trivalent cations are accommodated (Zanetti et al., 2004; Tuff and O'Neill, 2010). Elevated Ti concentrations in olivine are also thought to may be explained by microinclusions (Bussweiler et al., 2015). The Ti distribution coefficient between olivine and silicate melt lies within the range of 0.005–0.016 and can increase with decrease Mg# of the olivine (Tuff and O'Neill, 2010; Bussweiler et al., 2015).

The reason for difficulties of Zr and particularly Nb accommodation in olivine is their low distribution coefficients, which are D_{Zr}, $D_{Nb} \ll 1$ and $D_{Zr} > D_{Nb}$ (0.001–0.0001 and lower) for both carbonate–silicate and carbonate-rich liquids (Girnis et al., 2013;

Table 7. Oxygen isotopic composition of olivine and orthopyroxene hosted in kimberlite and peridotite xenoliths

Sample	Mineral	Rock	Pipe	Color of mineral	Mg# of mineral, average	$\delta^{18}O$
Gr-14	Olivine	Garnet harzburgite, xenolith	Grib pipe	Colorless	0.91	5.17
Gr-14	Clinopyroxene	Garnet harzburgite, xenolith	Grib pipe		0.93	6.08
13Gr-1-749-6-1	Olivine	Garnet lherzolite, xenolith	Grib pipe	Colorless	0.92	5.09
13Gr-1-749-6-1	Orthopyroxene	Garnet lherzolite, xenolith	Grib pipe	Colorless	0.93	5.18
13Gr-1-749-754	Olivine	Kimberlite	Grib pipe	Colorless	0.93	5.64
13PN1490-1450	Olivine	Kimberlite	Pionerskaya pipe	Yellow	0.92	5.26
13PN1490-1450	Olivine	Kimberlite	Pionerskaya pipe	Colorless	0.92	5.34

Petrographic characteristics of xenoliths are given in (Sazonova et al., 2015).

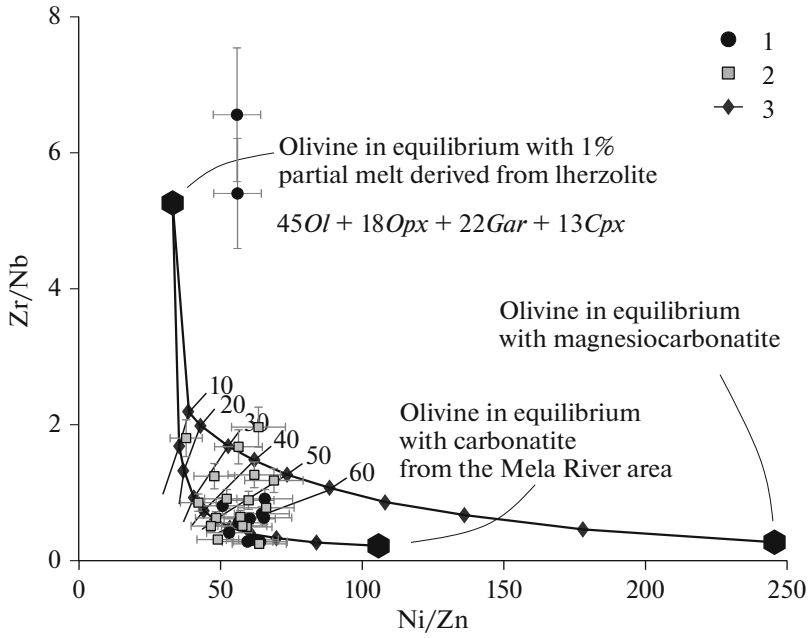

Fig. 9. Zr/Nb–Ni/Zn for olivine in kimberlite. The diagram shows isopleths of olivine in equilibrium with melts formed by mixing 1% partial melt derived from lherzolite, magnesiocarbonatite (Achterbergh et al., 2002), and carbonatite in carbonatite–kimberlite sills in the Mela River area, Arkhangelsk diamond province (Pervov et al., 2005b). Numerals on the right side of the line show the percentage of the carbonatite component in the mixture. Olivine: (1) macrocrysts from the Grib pipe; (2) macrocrysts B hosted in kimberlite from the Pionerskaya pipe; (3) model compositions in equilibrium with mixture of partial melts derived from lherzolite and carbonatite. The phase composition of lherzolite is according to (Girnis et al., 2013), element concentrations in lherzolite are assumed as in PM (McDonough and Sun, 1995), melt is assumed to be equilibrium one, the distribution coefficients are from (Girnis et al., 2013) and, for Zn, from (Davis et al., 2013), concentrations of elements in carbonatite from carbonatite–kimberlite sills in the Mela River are from (Pervov et al., 2005b). The distribution coefficients of elements between olivine and melt are assumed according to (Girnis et al., 2013) for the silicate liquid and according to (Dasgupta et al., 2009; Sweeney et al., 1994) for carbonatite melt; the distribution coefficients used in the calculations are weighted mean values.

Dasgupta et al., 2009; Sweeney et al., 1995; Zanetti et al., 2004; Bussweiler et al., 2015).

Carbonate-rich melts and carbonatite are, unlike silicate liquids, significantly enriched in Nb relative to Zr, as follows from $D_{Zr} < D_{Nb}$ between carbonate and silicate liquids and from data on natural carbonatites related to ultramafic magmatism. The Nb and Zr distribution coefficients between carbonate and silicate liquids were estimated at 0.503 and 0.016, respectively (P = 0.8–0.9 GPa, T = 965–1015°C, Veksler et al., 1998). For anhydrous systems at P = 1.0–1.7 GPa and T = 1220–1240°C, these coefficients are 0.39–0.73 for Nb and 0.06–0.28 for Zr. For hydrous systems at P = 1.7–3.0 GPa and T = 1150–1200°C, the coefficients are 0.51–1.16 and 0.12–0.56 for Nb and Zr, respectively (Martin et al., 2013). Natural carbonatites possess Zr/Nb = 0.6–0.8 on average (Chakhmouradian, 2006) and sometimes contain up to 3000–12 230 ppm Nb and 550–5410 ppm Zr (Woolley and Kempe, 1989; Chakhmouradian, 2006). The Zr/Nb ratio of carbonatite in carbonatite–kimberlite sills in the Mela River area in the Arkhangelsk province varies from 0.11 to 0.47 (Pervov et al., 2005b).

The distribution of these elements in deep-sitting carbonate fluid may be reflected in the composition of clinopyroxene-hosted Mg-carbonatite inclusion in lherzolite, whose crystallization depth was estimated at 200 km and whose Zr/Nd is close to 0.2 (Achterbergh et al., 2002).

This led us to believe that the variations in the Zr/Nb ratio of our olivine may reflect its interaction with melt/fluid containing variable percentage of a carbonate component. Figure 9 presents a diagram illustrating the composition of olivine in equilibrium with mixtures of 1% partial melts from lherzolite with high garnet and clinopyroxene contents (Girnis et al., 2013), for which a PM composition (McDonough and Sun, 1995) was assumed, and magnesiocarbonatite. The latter was assumed to have either (1) the composition of the clinopyroxene-hosted inclusion from lherzolite (Achterbergh et al., 2002) or (2) the average composition of carbonatites in sills at the Mela River in ADP (Pervov et al., 2005b). The composition points of low-Ti olivine in kimberlite from the Grib pipe define a compact group corresponding to a high percentage of the carbonate component.

The known distribution coefficients of certain elements (Bussweiler et al., 2015; Davis et al., 2013;

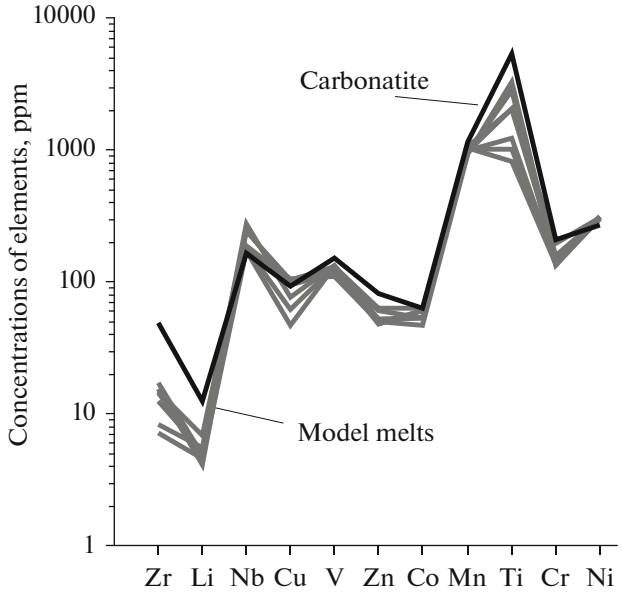

Fig. 10. Concentrations of minor admixtures in the model melt in equilibrium with olivine hosted in kimberlite from the Grib pipe in comparison with the concentrations in 0.03% partial melt of carbonatite composition derived peridotite, according to (Dasgupta et al., 2009). See Table 8 for parameters used to calculate the model melts and carbonatite partial melt.

Dasgupta et al., 2009, Girnis et al., 2013) make it possible to calculate the concentrations of these elements in melts in equilibrium with olivine (Table 8). The model composition of melt in equilibrium with the low-Ti olivine in kimberlite from the Grib pipe is closely similar (Table 8, Fig. 10) to 0.03% partial carbonatite melt derived from garnet lherzolite, as calculated in (Dasgupta et al., 2009).

The composition points of high-Ti macrocrysts B hosted in kimberlite from the Pionerskaya pipe are significantly scattered relative to the mixing lines, which may suggest the effect of another source and/or another mechanism of their origin.

It has been demonstrated in (Sweeney et al., 1995) that partial melts derived from mantle peridotites metasomatized by carbonate melts should possess Ti/Na ratios lower than those of melts derived from a source metasomatized by silicate melts. These differences are inherited by olivine in equilibrium with the melts. Olivine from the Grib pipe has Ti/Nb = 0.05–0.23 (averaging at 0.14 ± 0.06, $n = 10$), whereas macrocrysts B from the Pionerskaya pipe possess Ti/Nb = 0.90–2.39 (averaging at 1.44 ± 0.44, $n = 19$), which may suggest a stronger effect of the carbonate component on olivine macrocrysts in the Grib pipe.

Oxygen isotopic composition of olivine and the role of the carbonate component. Olivine in metasomatized mantle peridotite xenoliths can display perceptible deviations of its $\delta^{18}O$ values (toward both greater and lower values) from those typical of normal peridotite mantle material ($\delta^{18}O = 5.18 \pm 0.28‰$, Mattey et al., 1994). The $\delta^{18}O$ variations of olivine span a range of 1.3‰ and do not extend above 5.6‰: 4.9–5.6‰ (Rehfeldt et al., 2008), 5.3–5.4‰ (Perkins et al., 2006), and 4.3–5.6‰ (Zhang et al., 2000). Kimberlite-hosted olivine from the Grib pipe has an oxygen isotopic composition close to the upper limit of the ranges, while the oxygen isotopic composition of olivine macrocrysts in kimberlite from the Pionerskaya pipe corresponds to the "mantle" range (Table 7, Fig. 11). Not only the significant variations in the $\delta^{18}O$ values but also their correlations with Mg# of mantle minerals (olivine and clinopyroxene) were interpreted as suggesting the effect of mantle metasomatism. Correlations between $\delta^{18}O$ and Mg# of clinopyroxene in Cenozoic intraplate alkaline basalts in eastern China (Liu et al., 2015) were reported as resulting from the influence of melts derived from the oceanic crust of the stagnant Pacific slab on the origin of the basalts. The elevated $\delta^{18}O$ values (>5.4‰) of olivine in OIB were explained by the effect of a EM2 source (Eiler,

Table 8. Concentrations (ppm) of minor elements in olivine hosted in kimberlite from the Grib pipe (average) and in model melts

Model melts and their calculation parameters	Zr	Li	Nb	Cu	V	Zn	Co	Mn	Ti	Cr	Ni
0.03% melt derived from peridotite, carbonatite	48	12	165	92	149	80	62	1127	5256	208	265
Kimberlite-hosted olivine from the Grib pipe, average	0.4	1.5	0.6	6.9	5.1	51	134	774	33	131	3028
Model melt	11	5	175	86	122	54	57	993	2198	137	303
Distribution coefficient (reference)	0.036 (4)	0.29 (3)	0.0036 (4)	0.08 (1)	0.042 (1)	0.96 (3)	2.37 (3)	0.78 (3)	0.015 (5)	0.96 (2)	10 (5)

References for distribution coefficients: (1) (Girnis et al., 2013); (2) (Bussweiler et al., 2015); (3) (Davis et al., 2013); (4) (Sweeney et al., 1995); (5) (Dasgupta et al., 2009); the composition of partial melt derived from peridotite is calculated using distribution coefficients from (Dasgupta et al., 2009; Girnis et al., 2013).

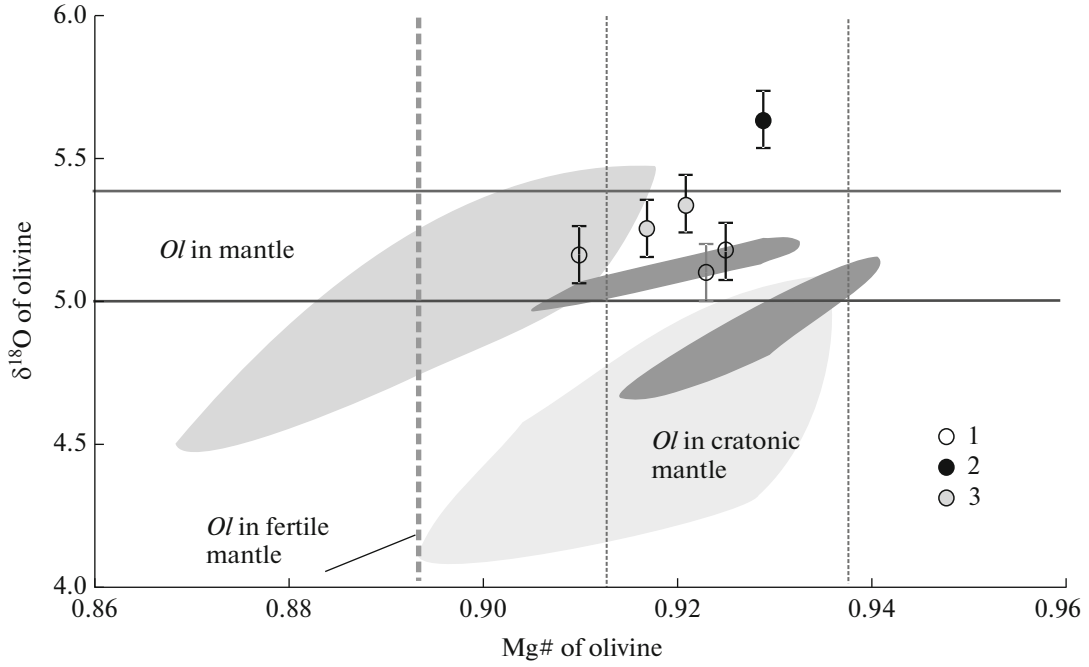

Fig. 11. $\delta^{18}O$–average Mg# diagram for olivine in kimberlites and peridotite xenoliths from the Grib and Pionerskaya pipes. (1) Olivine and orthopyroxene in peridotite xenoliths (garnet lherzolite and harzburgite) from the Grib pipe; (2) olivine in kimberlite from the Grib pipe; (3) olivine in kimberlite form the Pionerskaya pipe. Gray fields show the composition of olivine in polymictic peridotite xenoliths (polymictic breccia) hosted in kimberlite in Kimberley, South Africa (Zhang et al., 2000). Horizontal lines show the limits of the oxygen isotopic composition of mantle olivine $\delta^{18}O = 5.2 \pm 0.2‰$ (Mattey et al., 1994), and vertical lines constrain Mg# of olivine in cratonic peridotites (Menzies, 1990). The diagram also shows Mg# = 0.89 of olivine in the minimally depleted (fertile, pristine) mantle (Ionov et al., 2005). The error of Mg# (±0.1 mol) is smaller than the size of the symbols.

2001). The absence of oxygen isotopic equilibrium between olivine and clinopyroxene in wehrlite xenoliths was thought to be caused by mantle metasomatism under the effect of high-Si melts/fluids derived from subducted eclogites (Rehfeldt et al., 2008). The absence of isotopic equilibrium between minerals in eclogite xenoliths and the shift of $\delta^{18}O$ from typical mantle values toward heavier ones (for example, 5.72–8.24‰ for garnet) were interpreted as evidence of the effect of metasomatic agents, first of all, carbonatite melts/fluids (Huang et al., 2014).

Our earlier data on olivine in kimberlite from the Grib pipe (Sazonova et al., 2015) and the aforementioned geochemical data, including similarities between the melt that was in equilibrium with this olivine and carbonatite melts, suggest that a significant role in the origin of the olivine could be played by carbonate melt/fluid. We have estimated the role of carbonate fluid as an agent forming the isotopic parameters of olivine from the pipes. As a first-order proxy, metasomatic interaction between carbonatite melt and silicate material in the mantle can be approximated by a standard model, analogous to that in (Taylor, 1978), for fluid/rock interaction in an open system. The starting and final compositions of the "rock" can be assumed as "unaltered mantle" $\delta^{18}O$ values and those measured in the samples, respectively.

It is more difficult to select the starting parameters for the carbonate fluid. For the Grib pipe, we have measured the isotopic parameters of carbonates in kimberlite (Bogatikov et al., 2008), but these values likely rather characterize transformations during the late evolution of the kimberlite melt, and hence, as the desired estimates we assumed the composition of primary carbonatite melts (Taylor et al., 1967). Calculations indicate that the oxygen isotopic composition of the olivine could be formed at interaction with carbonatite (carbonate) fluid in the course of mantle metasomatism. In our calculations we assumed the model composition of a mantle rock consisting of 60% olivine and 40% pyroxene, the interaction temperature was assumed to be 1000°C, and the coefficients of equilibrium fractionation of oxygen isotopes in the carbonate–mineral were taken up according to the systematics (Chacko et al., 2001). Our estimates indicate that interaction between mantle minerals and carbonate fluid whose isotopic–geochemical parameters lie within the compositional ranges of mantle carbonatites is able to give rise to significant variations in $\delta^{18}O$ olivine and result in isotopic compositions either heavier or lighter than the conventionally assumed "mantle" parameters (Fig. 12). The variations in $\delta^{18}O$ of olivine can be from 4 to 7‰ depending on the composition of the carbonate fluid.

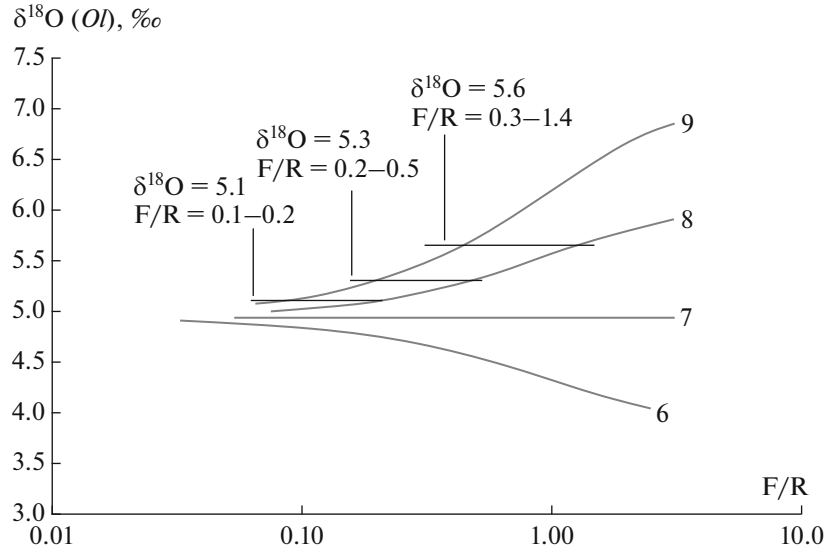

Fig. 12. Oxygen isotopic composition of olivine modified at interaction with carbonate fluid depending on the integral fluid/rock (F/R) ratio. The calculations were carried out with various $\delta^{18}O$ (from 6 to 9‰, numerals near the calculated lines) of the carbonate fluid. Horizontal lines correspond to $\delta^{18}O$ of olivine in peridotite xenoliths ($\delta^{18}O = 5.1$‰) and kimberlite from the Grib pipe ($\delta^{18}O = 5.3$ and $\delta^{18}O = 5.6$‰).

The calculations for our olivine samples from pipes in the Arkhangelsk province demonstrate that interaction with carbonate fluid may have occurred in an open system, for example, when carbonatite melt percolated through domains in mantle rocks. The elevated $\delta^{18}O$ values of our olivine samples from the Grib pipe indicate that $\delta^{18}O$ of the carbonate melt was about 8–9‰. The estimated fluid/rock (F/R) ratio differs for olivine in different settings. When olivine of the peridotite xenoliths ($\delta^{18}O \approx 5.1$‰) was formed, the F/R ratio could be at a minimum (0.1–0.2), while this ratio for kimberlite olivine in the Pionerskaya and Grib pipes ($\delta^{18}O \approx 5.3$ and $\delta^{18}O \approx 5.6$‰) could be 0.2–0.5 and 0.2–1.4, respectively. The high F/R ratio of olivine from the Grib pipe may reflect a high degree of interaction with carbonate fluid.

Olivine macrocrysts from the Grib pipe could thus be formed at more intense participation of carbonate fluid than during the origin of olivine in peridotite xenoliths in the Pionerskaya pipe, with this conclusion consistent with the above estimates derived from geochemical data.

Ni, Zn, and Cu in Olivine Hosted in Kimberlite from the Grib Pipe and the Role of the Sulfide Phase

The Cu/Zn ratio of olivine in xenoliths and kimberlite can significantly vary (Fig. 6a). In our olivine samples from the Grib pipe, some olivine grains are significantly enriched in Cu while others contain much less of this element (the Cu concentrations vary from 2.4 to 8.1 ppm), whereas the Zn concentrations remain almost unchanging (52–74 ppm). An important role in distributing Ni, Zn, and Cu when the mantle source was melted may have been played by a sulfide phase, because the chemical affinity of these elements with sulfur is different, and the distribution coefficients between the sulfide and silicate liquids are 800–1000 for Cu (Ripley et al., 2002; Barnes and Maier, 1999) or 900–1000 near QFM (Li and Audetat, 2012). These coefficients are 300 for Ni (Barnes and Maier, 1999) or decrease from 1300 to 200 with increasing oxygen fugacity (Li and Audetat, 2012) and are 0.28–0.94 for Zn (Lee et al., 2012). The affinity of these elements to sulfide (monosulfide solid solution *mss*) is as follows: the distribution coefficient between sulfide and silicate liquids is 180–450 for Cu at QFM – 1; varies between 800 and 300 with increasing oxygen fugacity for Ni; and insignificantly varies about one for Zn (Lee et al., 2012). Obviously, the transition of Ni, Zn, and Cu into silicate liquid when a mantle source is melted depends on the proportion of the sulfide phase *mss* and sulfide liquid.

Low-Ti olivine from the Grib pipe typically shows Cu/Zn ratios varying from 0.29 to 0.06 at insignificantly varying Mg# (0.92–0.93; Fig. 13a) and Ni concentrations (from 2950 to 3100 ppm). Significantly decreasing Cu/Zn ratios in olivine may suggest that the melt was depleted in Cu and (much less significantly) in Zn. This behavior of the elements can be controlled by a phase whose Cu distribution coefficients is high and that for Zn is close to one. Such a phase could be sulfide, which was *mss*, with regard for the crystallization parameters of olivine macrocrysts in kimberlite from the Grib pipe (Kostrovitsky et al., 2004; Golubkova et al., 2013). Along with a high Cu

distribution coefficients, the sulfide is also characterized by a high Ni distribution coefficient, and the extent of melt depletion in this element should also depend on olivine crystallization. The equilibrium Ni/Fe distribution coefficient between olivine and equilibrium sulfide is (Fleet and Stone, 1990)

$$K_{D_3} = (X_{NiS}/X_{FeS})\left(X_{FeSi1/2O_2}/X_{NiSi1/2O_2}\right). \quad (1)$$

The K_{D_3} values at high temperatures (900–1400°C) and oxygen fugacity under mantle parameters insignificantly increase from 29 to 35 (according to experimental data) at an average of 32 (Fleet and Stone, 1990).

The Cu/Zn ratio of olivine hosted in kimberlite from the Grib pipe is not correlated with the Mg# and Ni concentration of the olivine ($R^2 = 0.001$ and 0.04, respectively). However, the (X_{NiS}/X_{FeS}) values for hypothetical sulfide in equilibrium with olivine calculated from the equilibrium K_{D_3} (30–34) and a known olivine composition do correlate with the Cu/Zn ratio of olivine ($R^2 = 0.91$–0.84, Fig. 13b). The (X_{NiS}/X_{FeS}) values within the range of 1.61–1.65 for the hypothetical sulfide correspond to approximately 63 mol % NiS in this sulfide, which in turn, corresponds to the composition of sulfides in equilibrium with magnesian olivine in kimberlites (Fleet and Stone, 1990). We believe that the strong correlation between the Cu/Zn ratio of the olivine and its Ni–Fe parameters, which depended on the simultaneously crystallizing sulfide phase, suggests that the Ni, Cu, and Zn distribution in olivine hosted in kimberlite from the Grib pipe was controlled (among other factors) by the crystallization of a sulfide phase *mss*.

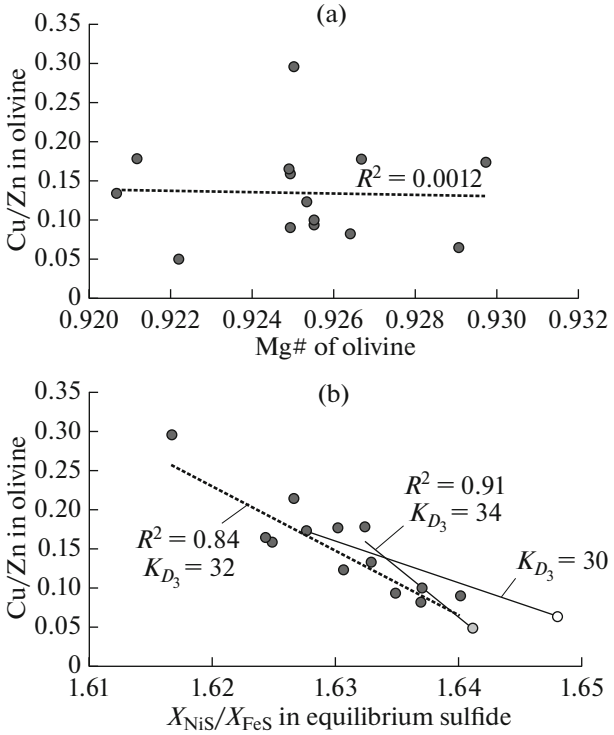

Fig. 13. Diagrams (a) Cu/Zn–Mg# of olivine and (b) Cu/Zn of olivine –X_{NiS}/X_{FeS} in hypothetical sulfide for Ti-poor olivine hosted in kimberlite from the Grib pipe. The X_{NiS}/X_{FeS} ratio of the hypothetical sulfide is calculated for $K_{D_3} = (X_{NiS}/X_{FeS})\left(X_{FeSi1/2O_2}/X_{NiSi1/2O_2}\right) =$ 0.30, 0.32, and 0.34 according to (Fleet and Stone, 1990). The strong correlation (0.84–0.91) between the Cu/Zn ratio of the olivine and the Ni–Fe parameters of its composition, which depended on the simultaneously crystallizing sulfide phase, suggest that an important factor controlling the Ni, Cu, and Zn concentrations in olivine hosted in kimberlite from the Grib pipe was simultaneous crystallization of the sulfide phase *mss*.

Role of Pyroxenite Partial Melts in the Origin of Kimberlite of the Pionerskaya Pipe

Zoning of olivine macrocrysts from the Pionerskaya pipe and the succession of interaction episodes with the proto- and kimberlite melts/fluids. A zoned distribution of major admixtures was documented in this mineral from various rocks, including kimberlite (Kopylova et al., 2007; Kamenetsky et al., 2008; Brett et al., 2009; Arndt et al., 2010; Pilbeam et al., 2013; Sobolev et al., 2015; Sazonova et al., 2015; Cordier et al., 2015; and references therein). Summarizing literature data on olivine zoning in kimberlites, we would like to mention the following facts. All olivine crystals (both macrocrystic olivine I and phenocrystic olivine II) bear outermost zones up to 100 μm thick (occasionally thicker; such zones are fragmentarily preserved in macrocrysts) that are richer in Fe than the cores of these grains; the forsterite content in the outer zone usually varies insignificantly and is close to 0.90–0.88, and these zones are much poorer in Ni and richer in Mn. Practically all researchers believe that the outer zones of olivine grains are formed when this mineral interacts with kimberlite melt. The outermost outer zones are of complicated structure and consist of transition zones, intermediate margins, and outermost rims. The margins are formed when the olivine interacts with percolating fluid, a process associated with the dissolution of orthopyroxene during pre-kimberlite deformation of lithospheric peridotites (Cordier et al., 2015). The rims are produced when the mineral crystallizes in kimberlite melt (Cordier et al., 2015) or reacts with it, a process associated with the dissolution of orthopyroxene xenocrysts (Pilbeam et al., 2013; Sazonova et al., 2015). Moreover, the rims can be modified by relatively weak diffusion processes after olivine crystallization (Pilbeam et al., 2013; Cordier et al., 2015). According to (Sobolev et al., 2015), the complicated structure of the olivine outer zones suggests fast changes in the parameters of the growth and dissolution processes during kimberlite evolution. The fast ascent of kimberlites is favorable for preserving concentration profiles. The cores of both the macro-

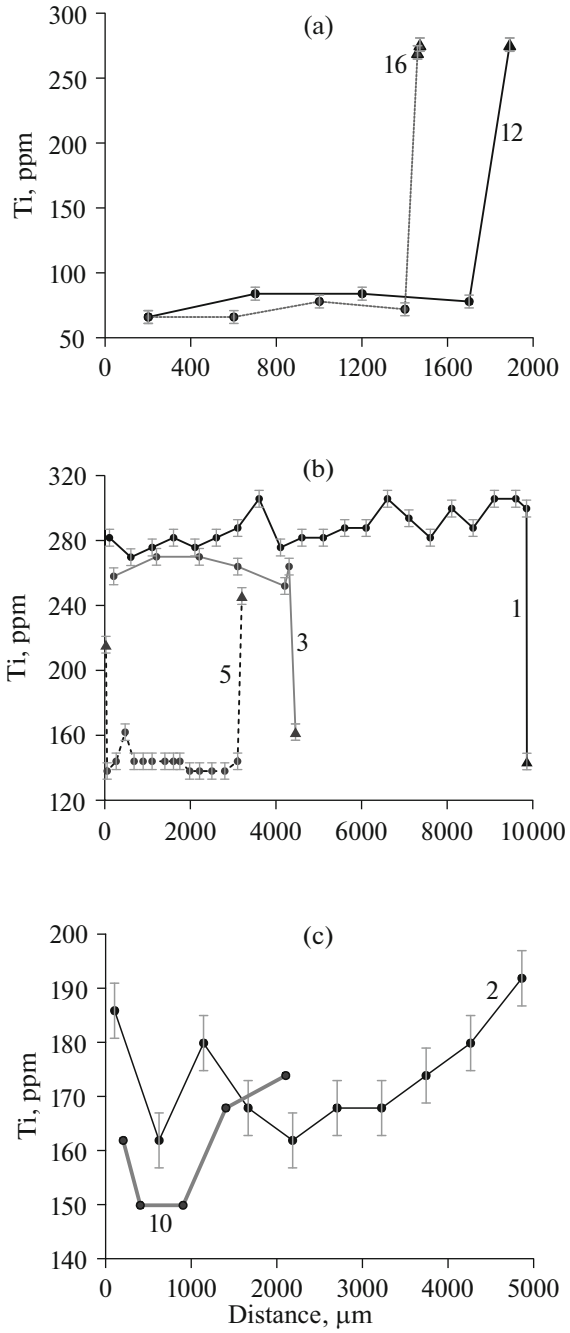

Fig. 14. Concentration profiles of Ti in olivine macrocrysts hosted in kimberlite from the Pionerskaya pipe. (a, b) Zoned Ti distribution between the core and outer zone of olivine macrocrysts: in macrocrysts A, Ti concentration increases in the outer zone if Ti concentration in the core is low or mildly high (grains 12 and 16 in Fig. 14a); in macrocrysts B, Ti concentration in the outer zone decreases if Ti concentration in the core is high (grains 1 and 3 in Fig. 14b) and increases if Ti concentration in the core is mildly high (Fig. 14b, grain 5); (c) U-shaped Ti concentration profile in macrocrysts B (grains 2 and 10 in Fig. 14c). Bars correspond to the analytical errors. See Table 6 for grain analyses. Numerals near the profile indicate the numbers of the grains.

crysts and the phenocrysts are homogeneous, without any significant variations in the concentrations of minor elements and with flat concentration profiles (Cordier et al., 2015; Sobolev et al., 2015; and others). However, Mg# and the concentrations of minor elements can broadly vary in certain zones (Sobolev et al., 2015; Sazonova et al., 2015; Cordier et al., 2015).

Titanium is an element particularly important when the zoning of olivine crystals is to be interpreted. As was pointed out in (Sobolev et al., 2015), "correlations between the concentration of a Ti admixture in olivine and its Mg# (content of forsterite) are the best criterion for distinguishing between olivine in various assemblages in kimberlites". This also follows from our results obtained on olivine in kimberlite and peridotite xenoliths (Sazonova et al., 2015; Kargin et al., 2016).

Data on zoning in olivine from the Pionerskaya pipe also indicate that Ti is a highly informative element in this context of olivine zoning (Fig. 14).

It was demonstrated in (Cherniak and Liang, 2014) that the Ti diffusion coefficient in olivine is much lower (by four to five orders of magnitude) than the diffusion coefficients of Mg–Fe and Ni in this mineral. This means that while the distribution of bivalent cations in olivine approaches equilibrium, i.e., becomes homogeneous, a zonal Ti distribution can still be preserved.

The distribution of Ti in the outer zones of macrocrysts depends on the level of Ti concentration in the cores: if it is no higher than 200 ppm, Ti concentration in the outer zone increases, and if the concentration in the core is higher than 200 ppm, Ti concentration in the outer zone decreases (Figs. 14a, 14b). These relations between Ti concentrations in the cores and outer zones reflect interaction between the olivine cores and kimberlite melt/fluid (which was responsible for the origin of the outer zone), when the core tended toward equilibrium with the kimberlite melt/fluid. Obviously, the episode of interaction with this kimberlite melt/fluid that formed the zoned core–outer zone (episode 2) occurred after the episode of the metasomatic transformation of the olivine core (episode 1), which was responsible for the elevated Ti concentrations in the cores of the phenocrysts. We cannot rule out that the differences between the levels of Ti concentrations in the outer zones of macrocrysts A and macrocrysts B (Figs. 14a, 14b) reflect different episodes of interaction with the high-Ti melt/fluid.

The development of the U-shaped profile of Ti distribution in the cores of macrocrysts B (Fig. 14c) may suggest that the crystals became enriched in Ti by means of diffusion-controlled exchange with a Ti-rich phase, i.e., interacted with Ti-enriched melt/fluid at high temperatures and were afterward reequilibrated by diffusion with clinopyroxene (this would had resulted in a convex, bell-shaped concentration profile; Cherniak and Liang, 2014).

The diffusion-controlled Ti distribution in the macrocrysts B (i.e., the absence of equilibration of the concentrations), which was produced when the crystals interacted with the Ti-rich melt/fluid, suggests than no equilibrium distribution of concentrations have been reached. Time t needed to reach reequilibration (95% equilibrium distribution of the average concentration of an element) in a given mineral can be calculated by the formula

$$t = L^2/bD,$$

where L is the radius of the crystal (in m); b is a geometric factor, which is $b = 5$ for a sphere; and D is the diffusion coefficient $D = 3.72 \times 10^{-21}$ m^2 s^{-1} for $T =$ 1200°C (Cherniak and Liang, 2014). We assumed a diffusion coefficient corresponding to a high temperature because the freezing temperature of Ti diffusion in olivine grains 1000–3000 μm across is close to 1150°C, and the initial temperature is approximately 1300°C (Cherniak and Liang, 2014).

For a crystal whose L = 1500–5000 μm, the time t should be 4 to 13 Ma at T = 1200°C. Our estimates imply that episode 1, a thermal event related to interaction with Ti enriched melt/fluid, occurred very shortly after the macrocrysts were entrapped by the kimberlite melt, no later than 13 Ma before the emplacement of the kimberlite.

The differences between Mg# and the concentrations of Ti and other minor elements between the core of macrocrysts B of episode 1 are much greater than the variations in these values within the core of any given individual macrocryst (Fig. 7). The Mg# of the cores of macrocrysts B varies from grain to grain within the range of 0.90 to 0.93 (i.e., 4 mol %) and within the analytical errors (±0.1 mol %) in any given grain. The variations in the Ti concentrations within any given grain core do not exceed 22%, and the differences between the cores of different grains are as great as 43%. The variations in the Ni concentration are within 4% in individual grains (a single grain shows variations within 7%) and up to 30% between the averages for individual grains.

The significantly different compositions of the cores of macrocrysts were described in much detail for olivine hosted in kimberlite in the Kangamiut area, Greenland (Cordier et al., 2015) and olivine from the Udachnaya pipe, Yakutia, which possess high (>150 ppm) and significantly varying (up to 300 ppm) Ti concentrations (Sobolev et al., 2015). Researchers who discussed the occurrence of olivine macrocrysts with variable forsterite mole fractions and concentrations of Ni, Mn, Ca, and other admixtures (regretfully, no data on the Ti concentrations are reported) (Cordier et al., 2015; Brett et al., 2009; Moore, 2012; Arndt et al., 2010; Jacobs, 2012) believe that the macrocrysts were formed when the peridotite source material was affected by percolating melt/fluid, a process that was associated with orthopyroxene dissolution and the origin of metasomatic dunite. This mechanism was experimentally reproduced for alkaline basalt melts at P = 1 GPa and T = 1300°C (Tursack and Liang, 2012). It was suggested (Cordier et al., 2015) that the melts/fluids could be rich in the carbonate component. According to (Kopylova et al., 2009; Moore, 2012), the agents of the early metasomatism were protokimberlite melts. It was also suggested (Sobolev et al., 2015) that Ti-rich olivine was produced during the early origin and evolution of kimberlite melt.

We employ olivine hosted in kimberlite from the Pionerskaya pipe to discuss the possible nature of melts responsible for the high Ti concentrations in the mineral.

The Zn/Cu ratio of olivine in kimberlite from the Pionerskaya pipe. As was mentioned above, the Zn/Cu ratios of olivine macrocrysts from the Grib and Pionerskaya pipes are different (Fig. 8b). This ratio is at a minimum in kimberlite-hosted olivine from the Grib pipe, in which the behavior of these elements could be controlled by the sulfide phase (see above). The maximum Zn/Cu ratios were found in olivine in kimberlite from the Pionerskaya pipe, with the highest values typical of macrocrysts B. Their Zn/Cu ratio is higher because of, first, the lower Cu concentrations (compare 7.5–1.4 ppm Cu in macrocrysts A and 4.7–0.8 ppm in macrocrysts B) and, second, higher Zn contents (37–55 and 43–61 ppm Zn in macrocrysts A and B, respectively). Thereby macrocrysts A are richer in Ni: 2915–3170 ppm in macrocrysts A and 2350–3120 ppm in macrocrysts B.

Nickel, zinc, and copper are characterized by different compatibility with olivine. Nickel is known to be highly compatible with this mineral, its concentrations in olivine are higher than in PM, and hence, this element continues to be compatible when mantle sources are melted (De Hooge et al., 2010).

The Zn distribution coefficient between olivine and silicate melt (at P = 1.5–2.0 GPa and T = 1300–1500°C) is 1.04 ± 0.12 (Le Roux et al., 2010), and values close to unity were obtained in (Bussweiler et al., 2015; Davis et al., 2013), i.e., Zn concentration in olivine should be close to that in the melt. The Cu distribution coefficient between olivine and silicate or carbonate–silicate melt is 0.048–0.08 (at $P > 1$ GPa and T = 1300–1450°C, Lee et al., 2012; and 6–12 GPa, Girnis et al., 2013); but this coefficient was estimated at 0.5 in Bussweiler et al., 2015), i.e., Cu is an incompatible element, which enriches the melt (and other silicate phases; Lee et al., 2012) until saturation with respect to sulfur is reached at given P, T, and f_{O_2} and sulfide phases appear (see above).

Data on Zn and Cu distribution between olivine and the groundmass of alkaline ultramafic rocks (Arzamastsev et al., 2009) validate the above experimental results on the distribution coefficients: the distribution coefficients are 0.01–0.03 for Cu and 0.36–1.39 for Zn.

Table 9. Composition of garnet–pyroxene xenoliths from the Grib pipe

Component	Sample 14Gr1-903-1	Sample 13Gr1-569-575-5
SiO_2	46.00	46.38
TiO_2	0.18	0.52
Al_2O_3	10.72	4.43
Fe_2O_3	5.59	13.69
MnO	0.205	0.234
MgO	20.97	18.85
CaO	10.98	9.89
Na_2O	0.98	0.73
K_2O	0.50	0.18
P_2O_5	0.04	0.05
S	0.05	0.05
LOI	3.08	3.78
Cr	2358	2096
V	242	107
Co	140	84
Ni	681	961
Cu	13	33
Zn	118	199
Rb	19	2
Sr	239	74
Zr	22	53
Ba	640	53
Y	7	23
Nb	3	6
vol %		
Cpx	60	70
Gar	40	30
mss	0.36	0.36

Major oxides were analyzed by XRF, minor and trace elements were determined by ICP-MS at IGEM; the content of sulfide *mss* in pyroxenite was assumed according to (Li and Audetat, 2012). Oxides are given in wt %, elements are in ppm.

The distribution of transition metals (Ni, Cu, and Zn) in olivine can be controlled by the following factors: (1) the presence of sulfides and their state; (2) the presence of Fe–Ti and Fe–Cr oxides (ilmenite and spinel), and (3) the presence of garnet and clinopyroxene in the residue/cumulate of the melt.

To explain the reasons for the very high Zn/Cu ratios (from 12 to 56 at an average of 28) in the Ti-rich macrocrysts B from the Pionerskaya pipe, it is interesting to analyze how the Zn/Cu ratio of the partial melts depends on the phase composition of the source material from which these melts were derived.

Experimental data on the distribution coefficients of some transition metals, Zn among others, for the basaltic system at $P = 1.5–2.0$ GPa and $T = 1300–1500°C$ show that melts derived from eclogite and pyroxenite should be richer in Zn (i.e., possess lower Mn/Zn and higher Zn/Fe ratios) than melts from peridotite sources, because the melting of olivine and orthopyroxene, dominant minerals of the latter sources, is not associated with any appreciable fractionation of transition elements, in contrast to the melting of clinopyroxene and garnet in pyroxenite/eclogite sources (Le Roux et al., 2010). The opposite effect can be caused, at low degrees of melting, by the occurrence of spinel in the residue, because this mineral is noted for a high Zn distribution coefficient of 5.2 ± 0.5 for basalt melt (at 3 GPa; Davis et al., 2013). The Cu distribution coefficients of olivine, garnet, and clinopyroxene are similar (Girnis et al., 2013; and others), and the distribution of this element is controlled, first of all, by the sulfide phase.

Data on garnet–clinopyroxene mantle xenoliths hosted in kimberlite in the Grib pipe show (Nosova et al., 2015) that some varieties of these xenoliths possess high Zn/Cu ratios (Table 9).

The Cu, Zn, Ni, and Ti proportions of the high-Ti macrocrysts B hosted in kimberlite from the Pionerskaya pipe plot close to the calculated composition of olivine in equilibrium with mix of partial melts derived from pyroxenite xenoliths and a hypothetical peridotite source (Fig. 15). These data led us to suggest that macrocrysts B in the Pionerskaya pipe may have been produced with the involvement of partial melts derived from a pyroxenite source, i.e., melts that were in equilibrium with garnet–pyroxene residue.

Garnet–clinopyroxene mantle rocks (mantle pyroxenites) are interpreted as: (1) high-pressure cumulates of mafic melts (Dawson, 1980; and others) or (2) mantle metasomatites, which were formed by interaction either between partial melts from eclogites with mantle peridotite (Yaxley and Green, 1998; Smart et al., 2009; and others) or between protokimberlite melt and host peridotite (Kopylova et al., 2009; Newton et al., 2016).

The aforementioned data on the composition of macrocrysts B and their zoning may be regarded as evidence of their metasomatic genesis under the effect of percolating melt/fluid, as follows from the fact that the composition varies from grain to grain. The metasomatic episode likely took place shortly before the kimberlite was emplaced, because the olivine preserves its U-shaped profile of Ti distribution. These considerations led us to suggest that, if the olivine with a high Zn/Cu ratio was formed with the participation of partial melts from pyroxenite, the pyroxenite source could be related to the protokimberlite melts. However, constructive discussion of the nature of this

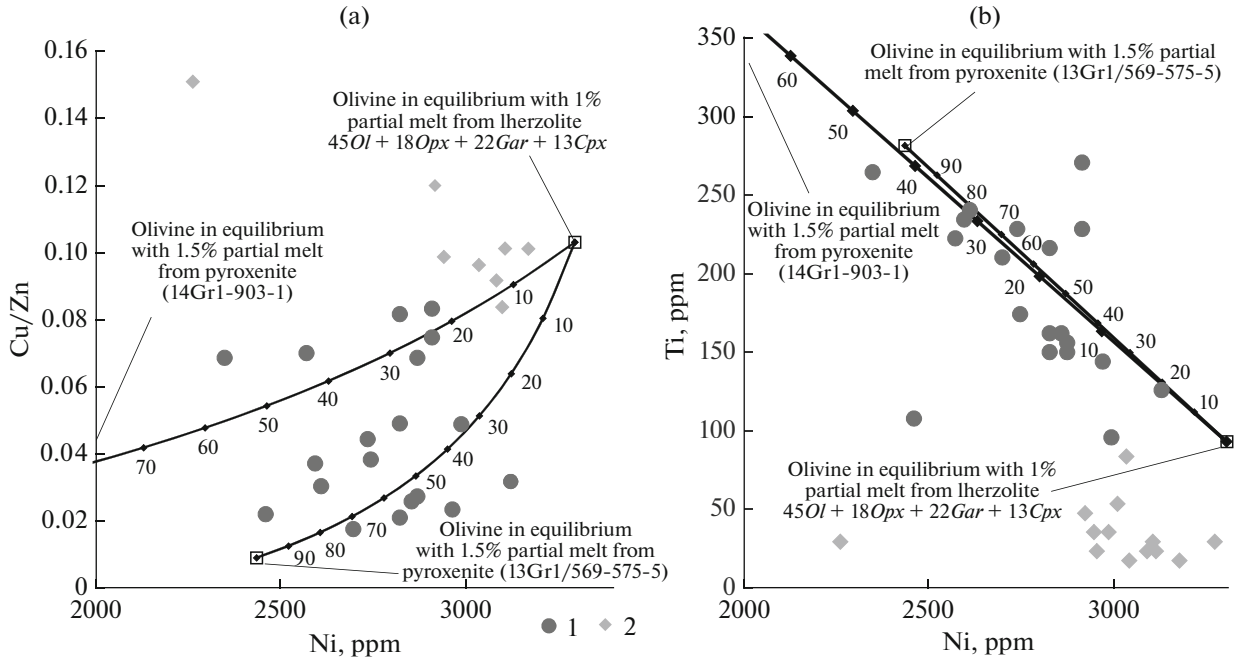

Fig. 15. Diagrams (a) Cu/Zn–Ni and (b) Ti–Ni for olivine hosted in kimberlite from the Pionerskaya pipe. Olivine: (1) macrocrysts B; (2) macrocrysts A. The diagram shows isopleths of olivine in equilibrium with melts formed by mixing 1% partial melt derived from lherzolite, and 1.5% partial melt derived from garnet clinopyroxenite (sample 14Gr1-903-1), and garnet clinopyroxenite (sample 13 Gr1-569-575-5). Numerals near the line correspond to the percentage of the partial melt from pyroxenite. Compositions of xenoliths of garnet clinopyroxenites are listed in Table 9. Parameters for calculating melt derived from lherzolite are given in captions to Fig. 9. The following distribution coefficients were assumed to calculate the pyroxenite partial melt: 0.0035 and 0.043 for Cu (Lee et al., 2012), 0.89 and 0.68 for Zn (Pertermann et al., 2004), 0.3 and 4 for Ni (Pertermann et al., 2004; Girnis et al., 2013), and 0.262 and 0.124 for Ti (Davis et al., 2013). The distribution coefficients for sulfide are 307 for Cu, 0.3 for Zn, and 300 for Ni according to (Li and Audetat, 2012).

pyroxenite source requires additional data, first and foremost, isotopic ones.

Macrocrysts A are noted for high Mg# (from 0.91 to 0.93), low Ti concentrations (<70 ppm), and high Ni contents (2900 ppm on average). These geochemical parameters are comparable with those of olivine in garnet harzburgite xenoliths in the Grib pipe (Sazonova et al., 2015), and this makes it possible to regard them as xenocrysts.

Differences between Kimberlites in the Grib and Pionerskaya Pipes and Olivine in Them

Mineralogical and geochemical traits of kimberlites in the Grib pipe are similar to those of archetypical kimberlites of group I, whereas kimberlites from the Pionerskaya pipe exhibit mineralogical and geochemical similarities with group-II kimberlites, referred to as orangeite (Figs. 4, 5).

According to (Kononova et al., 2007; Mahotkin et al., 2000; Parsadanyan et al., 1996), the Nd isotopic composition of kimberlite from the Grib pipe corresponds to $\varepsilon_{Nd}(T)$ from +0.9 to +0.5, whereas kimberlite from the Pionerskaya pipe yields $\varepsilon_{Nd}(T)$ from –2.3 to –4.4 (within the depth ranges corresponding to our samples). With regard for the Sr and Pb isotopic composition of the rocks, these differences in the Nd isotopic composition make it possible (Beard et al., 2000) to classify kimberlites in the Zolotitskoe field (including kimberlite in the Pionerskaya pipe) with a geochemical type transitional between group-I kimberlites and group-II kimberlites/lamproites; these rocks were ascribed to kimberlites of group II in (Parsadanyan et al., 1996). Kimberlites from the Grib pipe affiliate with group I of kimberlites (Kononova et al., 2007).

According to the currently prevailing viewpoint, the partial melts of kimberlite could contain both CO_2 and H_2O and were carbonate–silicate liquids in which melt containing less than 15–20 wt % SiO_2 is stable within a broad enough temperature range (Becker and Le Roex, 2006; Kopylova et al., 2007; Mitchell, 2008; Girnis et al., 2013; and others) or could be carbonate- or Na carbonate-rich melt, or else have a chloride–carbonate composition (Kamenetsky et al., 2008, 2014; Dasgupta, 2013; Litasov et al., 2013; Sharygin et al., 2015). The lamproite and group-II kimberlite melts were generated in the presence of geochemically enriched vein hydrous potassic associations (Becker and Le Roex, 2006; Foley, 1992; Giuliani et al., 2015; Mitchell, 1995).

Olivine macrocrysts in kimberlites from the Grib and Pionerskaya pipes differ in geochemical parameters and oxygen isotopic composition. As follows from the above considerations, the main differences may be explained by the role of the carbonate component in the genesis of olivine and likely also their host kimberlites. Our results suggest that the Ti-poor olivine macrocrysts from the Grib pipe possess geochemical features (low Ti/Na and Zr/Nb ratios and $\delta^{18}O$ values higher than the typical mantle ones) that can be interpreted as evidence that the olivine interacted with carbonate-rich melts/fluids. Conversely, the geochemical parameters of high-Ti olivine macrocrysts from the Pionerskaya pipe suggest higher contents of the silicate (hydrous silicate) component during their crystallization.

Our data on the olivine are generally consistent with differences between the geochemical parameters and isotopic compositions of kimberlites in the Grib and Pionerskaya pipes.

CONCLUSIONS

We obtained data on the geochemistry and oxygen isotopic composition of olivine from two kimberlite pipes in the Arkhangelsk diamond province: the Grib and Pionerskaya pipes. The mineralogy and geochemistry of kimberlite in the Grib pipe are similar to those of archetypical group-I kimberlite, and those of kimberlite from the Pionerskaya pipe are similar to group-II kimberlites (orangeites).

The geochemistry and isotopic parameters of dominant olivine macrocrysts in kimberlites from the two pipes are remarkably different. Olivine macrocrysts in kimberlite from the Grib pipe are dominantly highly magnesian (Mg# from 0.92 to 0.93), poor in Ti (Ti < 70 ppm), and possess low Ti/Na (0.05–0.23), Zr/Nb (0.28–0.80), and Zn/Cu (3–20) ratios, low Li concentrations (1.2–2.0 ppm), $\delta^{18}O$ = 5.64‰ that is higher than the mantle values ($\delta^{18}O = 5.18 \pm 0.28$‰, Mattey et al., 1994). Olivine macrocrysts from the Pionerskaya pipe are dominated by varieties with broadly varying Mg# (from 0.90 to 0.93) and with high Ti concentrations (100–300 ppm), high Ti/Na (0.90–2.39), Zr/Nb (0.31–1.96), and Zn/Cu (12–56) ratios, elevated Li concentrations (1.9–3.4 ppm), and $\delta^{18}O$ = 5.34‰, which corresponds to olivine in mantle peridotites.

The probable reasons for the principal differences in the olivine compositions may be related to the role of the carbonate component. Low-Ti olivine macrocrysts from the Grib pipe possess geochemical and isotopic characteristics that can be interpreted as evidence that this olivine interacted with carbonate-rich melts/fluids. This conclusion finds further support in the similarities between the geochemical parameters of the model melt in equilibrium with the low-Ti olivine and deep carbonatite melts (Dasgupta et al., 2009). Our calculations indicate that the variations in $\delta^{18}O$ of the olivine relative the "mantle" range can be fairly significant (either higher and lower than the "mantle" range) because of interaction with carbonate fluid, whose $\delta^{18}O$ do not extend outside the "carbonate box". In our calculations, we assumed that the system was open (Taylor, 1978) and the temperature was high (1000°C), and the calculated effects can readily account for the variations in $\delta^{18}O$ of olivine described herein and known from the literature (Fig. 13). The variations in $\delta^{18}O$ of the olivine generally span the range of 4 to 7‰ depending on the composition of the carbonate fluid. For olivine from the Grib pipe, the mass ratio of the carbonate fluid ($\delta^{18}O$ = 8–9‰) to metasomatized mantle rocks could be 0.2–1.4.

Olivine from the Grib pipe is noted for a strong enough correlation between the Cu/Zn and Ni–Fe parameters, which depended on the simultaneously crystallizing sulfide phase. We believe that this is an argument that the Ni, Cu, and Zn distribution in olivine from the Grib pipe was controlled during the crystallization of the sulfide phase *mss*.

Conversely, the geochemical parameters of high-Ti olivine macrocrysts from the Pionerskaya pipe suggest that the composition of this olivine was controlled by the silicate (hydrous silicate) component. This olivine is characterized by a zonal Ti distribution, with character of this distribution at the boundary between the cores of the olivine grains and their outer zones indicating that both the cores of the macrocrysts and their outer zones bear zoning independent from one another, and these types of zoning were generated when the mineral interacted with melt/fluid. The later episode, when the outer zone was formed, was most likely related to interaction of the kimberlite melt (Kopylova et al., 2007; Kamenetsky et al., 2008; Brett et al., 2009; Arndt et al., 2010; Pilbeam et al., 2013; Sobolev et al., 2015; Cordier et al., 2015). The compositional transformations of the macrocryst cores, which took place during an earlier episode, may have been of metasomatic nature and been triggered by melt/fluid percolating through the mantle source massif, as follows from the fact that the olivine composition varies from grain to grain. The metasomatic episode likely occurred shortly before the emplacement of the kimberlite.

Our calculations indicate that the composition of high-Ti macrocrysts hosted in kimberlite from the Pionerskaya pipe should correspond, in terms of Cu, Zn, Ni, and Ti proportions, to model olivine in equilibrium with mixture of partial melts derived from a pyroxenite source and from a peridotite source. It may be hypothesized that olivine phenocrysts in the Pionerskaya pipe were formed in the presence of melts derived from a pyroxenite source, whose nature is, however, uncertain.

ACKNOWLEDGMENTS

The authors thank V.G. Dryupin, I.S. Sagaidak, and the staff of the Territorial Collection of Geological Materials for the Northwestern Federal Okrug of the Russian Federation in Arkhangelsk; the corporate management of the Severalmaz OJSC and personally A.S. Galkin, I.S. Zezin, and A.N. Gudin for permission to collect kimberlite samples and assistance in this. We appreciate invaluable help in LA-ICP-MS analyses provided by V.K. Karandashev of the Institute of Microelectronic Technology and Ultrahigh-Purity Materials, Russian Academy of Sciences. Microprobe analyses of olivine were carried out by S.E. Borisovskii and E.V. Koval'chuk of the Institute of the Geology of Ore Deposits, Petrography, Mineralogy, and Geochemistry (IGEM), Russian Academy of Sciences. We thank the anonymous reviewer for constructive criticism that helped us to improve the manuscript. This study was financially supported by the Russian Foundation for Basic Research, project nos. 13-05-00644a, 16-05-00298a, and 15-05-03778a. The analytical work was partly financed under the Project "Geodynamic History of Lithospheric Growth in the Arkhangelsk Diamond Province as a Basis for Predicting the Diamond Potential of Kimberlites in the Arctic" of the Presidium of the Russian Academy of Sciences.

REFERENCES

Achterbergh, E., Griffin, W.L., Ryan, C.G., et al., Subduction signature for quenched carbonatites from the deep lithosphere, *Geology,* 2002, vol. 30, no. 8, pp. 743–746.

Arkhangel'skaya almazonosnaya provintsiya (Arkhangelsk Diamondiferous Province), Bogatikov, O.A., Eds., Moscow: Izd-vo MGU, 1999.

Arndt, N.T., Guitreau, M., Boullier, A.M., et al., Olivine and the origin of kimberlite, *J. Petrol.,* 2010, vol. 51, pp. 573–602.

Arzamastsev, A.A., Bea, F., Arzamastseva, L.V., and Montero, P., Trace elements in minerals as indicators of the evolution of alkaline ultrabasic dike series: LA-ICP-MS data for the magmatic provinces of Northeastern Fennoscandia and Germany, *Petrology,* 2009, vol. 17, no. 1, pp. 47–72.

Barnes, S-J. and Maier, W.D., The fractionation of Ni, Cu and the noble metals in silicate and sulfide liquids, Dynamic Processes in Magmatic Ore Deposits and their Application, in *Mineral Exploration,* Keays, R.R., Lesher, C.M., Lightfoot, P.C., and Farrow, C.E.G., Eds., *Geol. Assoc. Can., Short Course Notes*, 1999, vol. 13, pp. 69–106.

Batanova, V.G., Sobolev, A.V., and Kuzmin, D.V., Trace element analysis of olivine: high precision analytical method for JEOL JXA-8230 electron probe microanalyser, *Chem. Geol.,* 2015, pp. 149–157.

Beard, A.D., Downes, H., and Hegner, E., Mineralogy and geochemistry of Devonian ultramafic minor intrusions of the southern Kola Peninsula, Russia: implications for the petrogenesis of kimberlites and melilitites, *Contrib. Mineral. Petrol.,* 1998, vol. 130, pp. 288–303.

Beard, A.D., Downes, H., Hegner, E., et al., Geochemistry and mineralogy of kimberlites from the Arkhangelsk region, NW Russia: evidence for transitional kimberlite magma types, *Lithos,* 2000, vol. 51, nos. 1–2, pp. 47–73.

Becker, M. and Le Roex, A.P., Geochemistry of South African on- and off-craton, group I and group II kimberlites: petrogenesis and source region evolution, *J. Petrol.,* 2006, pp. 673–703.

Berry, A., Hermann, J., O'Neill, H.St.C., and Foran, G.J., Finger printing the water site in mantle olivine, *Geology,* 2007, vol. 33, pp. 869–872.

Bogatikov, O.A., Kononova, V.A., Nosova, A.A., and Kondrashov, I.A., Kimberlites and lamproites of the East European Platform: petrology and geochemistry, *Petrology,* 2007, vol. 16, no. 4, pp. 315–334.

Bogatikov, O.A., Kononova, V.A., Dubinina, E.O., et al., Nature of carbonates from kimberlites of the Zimnii Bereg Field, Arkhangelsk: evidence from Rb–Sr, C, and O isotope data, *Dokl. Earth Sci.,* 2008, vol. 420, no. 6, pp. 808–812.

Brett, R.C., Russell, J.K., and Moss, S., Origin of olivine in kimberlite: phenocryst or imposter, *Lithos,* 2009, vol. 1125, pp. 201–212.

Bussweiler, Y., Foley, S.F., Prelević, D., and Jacob, D.E., The olivine macrocryst problem: new insights from minor and trace element compositions of olivine from Lac de Gras kimberlites, Canada, *Lithos,* 2015, vol. 220–223, pp. 238–252.

Chacko, T., Cole, D.R., and Horita, J., Equilibrium oxygen, hydrogen and carbon isotope fractionation factors applicable to geological systems, in *Stable Isotope Geochemistry,* Valley J.W. and Cole D.R., Eds., *Rev. Mineral,* 2001, vol. 43, pp. 1–81.

Chakhmouradian, A.R., High-field-strength elements in carbonatitic rocks: geochemistry, crystal chemistry and significance for constraining the sources of carbonatites, *Chem. Geol.,* 2006, vol. 235, pp. 138–160.

Cherniak, D.J. and Liang, Y., Titanium diffusion in olivine, *Geochim. Cosmochim. Acta,* 2014, vol. 147, pp. 43–57.

Clement, C.R., A comparative geological study of some major kimberlite pipes in the Northern Cape and Orange Free State, *PhD thesis. University of Cape Town,* Cape Town, South Africa, 1982.

Coplen, T.B., Reporting of stable hydrogen, carbon, and oxygen isotopic abundances (Technical Report), *Pure Appl. Chem.,* 1994, vol. 66, pp. 707–712.

Cordier, C., Sauzeat, L., Arndt, N.T., et al., Metasomatism of the lithospheric mantle immediately precedes kimberlite eruption: new evidence from olivine composition and microstructures, *J. Petrol.,* 2015, vol. 56, no. 9, pp. 1775–1796.

Dasgupta, R., Hirschmann, M.M., McDonough, W.F., et al., Trace element partitioning between garnet lherzolite and carbonatite at 6.6 and 8.6 GPa with applications to the geochemistry of the mantle and of mantlederived melts, *Chem. Geol.,* 2009, vol. 262, pp. 57–77.

Dasgupta, R., Mallik, A., Tsuno, K., et al., Carbon–dioxide-rich silicate melt in the Earth's upper mantle, *Nature,* 2013, vol. 493, pp. 211–215.

Davis, F.A., Humayun, M., Hirschmann, M.M., and Cooper, R.S., Experimentally determined mineral/melt partitioning of first-row transition elements (FRTE) during partial melting of peridotite at 3 GPa, *Geochim. Cosmochim. Acta,* 2013, vol. 104, pp. 232–260.

Dawson, J.B., *Kimberlites and Their Xenoliths,* Berlin, Heidelberg: Springer Berlin Heidelberg, 1980.

De Hoog, J.C., Gall, L., and Cornell, D.H., Trace-element geochemistry of mantle olivine and application to mantle petrogenesis and geothermobarometry, *Chem. Geol.,* 2010, vol. 270, pp. 196–215.

Eiler, J.M., Oxygen isotope variations of basaltic lavas and upper mantle rocks, in *Stable Isotope Geochemistry, Rev. Mineral. Geochem.,* 2001, vol. 43, pp. 319–364.

Fleet, M.E. and Stone, W.E., Nickeliferous sulfides in xenoliths, olivine megacrysts and basaltic glass, *Contrib. Mineral. Petrol.,* 1990, vol. 105, pp. 629–636.

Foley, S., Vein-plus-wall-rock melting mechanisms in the lithosphere and the origin of potassic alkaline magmas, *Lithos,* 1992, vol. 28, pp. 435–453.

Foley, S.F., Prelevic, D., Rehfeldt, T., and Jacob, D.E., Minor and trace elements in olivines as probes into early igneous and mantle melting processes, *Earth Planet Sci. Lett.,* 2013, vol. 363, pp. 181–191.

Girnis, A.V., Bulatov, V.K., Brey, G.P., et al., Trace element partitioning between mantle minerals and silico-carbonate melts at 6–12 GPa and applications to mantle metasomatism and kimberlite genesis, *Lithos,* 2013, vol. 160–161, pp. 183–200.

Giuliani, A., Phillips, D., Woodhead, J.D., et al., Did diamond-bearing orangeites originate from MARID-veined peridotites in the lithospheric mantle?, *Nat. Commun,* 2015, vol. 6, p. 6837.

Golubkova, A.B., Nosova, A.A., and Larionova, Yu.O., Mg-ilmenite megacrysts from the Arkhangelsk kimberlites, Russia: genesis and interaction with kimberlite melt and postkimberlite fluid, *Geochem. Int.,* 2013, vol. 51, no. 5, pp. 421–441.

Hermann, J., O'Neill, H., and Berry, A., Titanium solubility in olivine in the system TiO_2–MgO–SiO_2: no evidence for an ultra-deep origin of Ti-bearing olivine, *Contrib. Mineral. Petrol.,* 2005, vol. 148, pp. 746–760.

Huang, J-X., Griffin, W.L., Greau, Y., et al., Unmasking xenolithic eclogites: progressive metasomatism of a key Roberts Victor sample, *Chem. Geol.,* 2014, vol. 364, pp. 56–65.

Ionov, D.A., Prikhodko, V.S., Bodinier, J.L., et al., Lithospheric mantle beneath the south-eastern Siberian Craton: petrology of peridotite xenoliths in basalts from the Tokinsky Stanovik, *Contrib. Mineral. Petrol.,* 2005, vol. 149, pp. 647–665.

Jacobs, D.A.B., Orthopyroxene stability within kimberlite magma: an experimental investigation, *MSc thesis, University of Stellenbosch,* 2012, p. 56.

Jochum, K.P., Weis, U., Stoll, B., et al., Determination of reference values for NIST SRM 610-617 glasses following ISO guidelines, *Geostand. Geoanal. Res.,* 2011, vol. 35, no. 4, p. 397.

Kamenetsky, V., Kamenetsky, M., Sobolev, A., et al., Olivine in the Udachnaya-East kimberlite (Yakutia, Russia): types, compositions and origins, *J. Petrol.,* 2008, vol. 49, pp. 823–839.

Kamenetsky, V.S., Golovin, A.V., Maas, R., et al., Towards a new model for kimberlite petrogenesis: evidence from unaltered kimberlites and mantle minerals, *Earth Sci. Rev.,* 2014, vol. 139, pp. 145–167.

Kargin, A.V., Sazonova, L.V., Nosova, A.A., et al., Sheared peridotite xenolith from the V. Grib kimberlite pipe, Arkhangelsk diamond province, Russia: texture, composition, and origin, *Geoscience Front.,* 2016. doi 10.1016/j.gsf.2016.03.001

Kargin, A.V., Nosova, A.A., Larionova, Yu.O., et al., Mesoproterozoic orangeites (kimberlites II) of West Karelia: mineralogy, geochemistry, and Sr–Nd isotope composition, *Petrology,* 2014, vol. 22, no. 2, pp. 151–183.

Kononova, V.A., Nosova, A.A., Pervov, V.A., and Kondrashov, I.A., Mesoproterozoic orangeites (kimberlites II) of West Karelia: mineralogy, geochemistry, and Sr–Nd isotope composition, *Dokl. Earth Sci.,* 2006, vol. 409, pp. 952–957.

Kononova, V.A., Golubeva, Yu.Yu., Bogatikov, O.A., and Kargin, A.V., Diamond resource potential of kimberlites from the Zimny Bereg Field, Arkhangel'sk Oblast, *Geol. Ore Deposits,* 2007, vol. 49, no. 6, pp. 483–505.

Kopylova, M.G., Matveev, S., and Raudsepp, M., Searching for parental kimberlite melt, *Geochim Cosmochim. Acta*, 2007, vol. 71, pp. 3616–3629.

Kopylova, M.G., Nowell, G.M., Pearson, D.G., and Markovic, G., Crystallization of megacrysts from protokimberlitic fluids: geochemical evidence from high-Cr megacrysts in the Jericho kimberlite, *Lithos,* 2009, vol. 112, Suppl. 1, pp. 284–295.

Kostrovitsky, S.I., Malkovets, V.G., Verichev, E.M., et al., Megacrysts from the Grib kimberlite pipe (Arkhangelsk province, Russia), *Lithos,* 2004, vol. 77, pp. 511–523.

Larionova, Yu.O., Sazonova, L.V., Lebedeva, N.M., et al., Age of kimberlites of the Arkhangelsk province: Rb–Sr, $^{40}Ar/^{39}Ar$ isotope-geochronological and mineralogical data on phlogopite, *Petrology,* 2016, vol. 24, pp. 562–593.

Le Roux, V., Lee, C.-T.A., and Turner, S.J., Zn/Fe systematics in mafic and ultramafic systems: implications for detecting major element heterogeneities in the Earth's mantle, *Geochim. Cosmochim. Acta,* 2010, vol. 74, pp. 2779–2796.

Lee, C.-T.A., Luffi, P., Chin, E.J., et al., Copper systematics in arc magmas and implications for crust–mantle differentiation, *Science,* 2012, vol. 336, pp. 64–68.

Li, Y. and Audetat, A., Partitioning of V, Mn, Co, Ni, Cu, Zn, As, Mo, Ag, Sn, Sb, W, Au, Pb, and Bi between sulfide phases and hydrous basanite melt at upper mantle conditions, *Earth Planet. Sci. Lett.,* 2012, vol. 355–356, pp. 327–340.

Litasov, K.D., Shatskiy, A., Ohtani, E., and Yaxley, G.M., Solidus of alkaline carbonatite in the deep mantle, *Geology,* 2013, vol. 41, no. 1, pp. 79–82.

Liu, J., Xia, Q.-K., Deloule, E., et al., Water content and oxygen isotopic composition of alkali basalts from the Taihang Mountains, China: recycled oceanic components in the mantle source, *J. Petrol.,* 2015, vol. 56, no. 4, pp. 681–702.

Mahotkin, I.L., Gibson, S.A., Thompson, R.N., et al., Late Devonian diamondiferous kimberlite and alkaline picrite (protokimberlite?) magmatism in the Arkhangelsk region, NW Russia, *J. Petrol.,* 2000, vol. 41, no. 2, pp. 210–227.

Martin, L.H.J., Schmidt, M.W., Mattsson, H.B., and Guenther, D., Element partitioning between immiscible carbonatite and silicate melts for dry and H_2O-bearing systems at 1–3 GPa, *J. Petrol.,* 2013, vol. 54, pp. 2301–2338.

Mattey, D., Lowry, D., and Macpherson, C., Oxygen isotope composition of mantle peridotite, *Earth Planet. Sci. Lett.,* 1994, vol. 128, pp. 231–241.

McDonough, W.F. and Sun, S.-S., Composition of the Earth, *Chem. Geol,* 1995, vol. 120, pp. 223–253.

Menzies, M.A., *Archaean, Proterozoic, and Phanerozoic lithosphere, Continental Mantle,* Menzies, M.A., Ed., Oxford: Oxford University Press, 1990, pp. 67–86.

Mitchell, R.H., *Kimberlites: Mineralogy, Geochemistry and Petrology,* New York: Plenum Press, 1986.

Mitchell, R.H., *Kimberlites, Orangeites and Related Rocks,* New York: Plenum Press, 1995.

Mitchell, R.H., Petrology of hypabyssal kimberlites: relevance to primary magma compositions, *J. Volcanol. Geotherm. Res.,* 2008, vol. 174, pp. 1–8.

Moore, A.E., Olivine: a monitor of magma evolutionary paths in kimberlite and olivine melilitites, *Contrib. Mineral. Petrol.,* 1988, vol. 99, pp. 238–248.

Moore, A.E., The case for a cognate, polybaric origin for kimberlitic olivines, *Lithos,* 2012, vol. 1–10, pp. 128–131.

Newton, D.E., Kopylova, M.G., Burgess, J., and Strand, P., Peridotite and pyroxenite xenoliths from the Muskox kimberlite, Northern Slave Craton, Canada, *Can. J. Earth Sci.,* 2016, vol. 53, no. 1, pp. 41–58.

Nosova, A.A., Sazonova, L.V., Larionova, Yu.O., et al., Protoliths of A-type mantle eclogites (garnet clinopyroxenites) from kimberlite xenoliths in the V. Grib pipe, Arkhangelsk Province, in *Petrografiya magmaticheskikh i metamorficheskikh gornykh porod. Materialy XII Vserossiiskogo Petrograficheskogo soveshchaniya s uchastiem zarubezhnykh* (Petrography of Magmatic and Metamorphic Rocks. Proceedings of 12th All-Russian Petrographic Conference with International Participation), Petrozavodsk: Karel'skii nauchnyi tsentr RAN, 2015, pp. 346–348.

Parsadanyan, K.S., Kononova, V.A., and Bogatikov, O.A., Sources of heterogeneous magmatism of the Arkhangelsk Diamondiferous Province, *Petrology,* 1996, vol. 4, no. 5, pp. 460–479.

Perkins, G.B., Sharp, Z.D., and Selverstone, J., Oxygen isotope evidence for subduction and rift-related mantle metasomatism beneath the Colorado Plateau–Rio Grande rift transition, *Contrib. Mineral. Petrol.,* 2006, vol. 151, pp. 633–650.

Pertermann, M., Hirschmann, M.M., Hametner, K., et al., Experimental determination of trace element partitioning between garnet and silica-rich liquid during anhydrous partial melting of MORB-like eclogite, *Geochem., Geophys., Geosyst.,* 2004, vol. 5, p. 1029. doi 10.1029/2003GC000638

Pervov, V.A., Bogomolov, E.S., Larchenko, V.A., et al., Rb–Sr age of kimberlites of the Pionerskaya Pipe, Arkhangel'sk Diamondiferous Province, *Dokl. Earth Sci.,* 2005a, vol. 400, no. 1, pp. 67–71.

Pervov, V.A., Larchenko, V.A., Stepanov, V.P., et al., Silly kimberlitov po r. Mela (Arkhangel'skaya almazonosnaya provintsiya): novye dannye o vozraste, sostave porod i mineralov, in *Geologiya almaza – nastoyashchee i budushchee* (Geology of Diamond—Present and Future), Voronezh: Voronezhskii gosuniversitet, 2005b.

Pilbeam, L.H., Nielsen, T.F.D., and Waight, T.E., Digestion fractional crystallization (DFC): an important process in the genesis of kimberlites. Evidence from olivine in the Majuagaa kimberlite, southern West Greenland, *J. Petrol.,* 2013, vol. 54, no. 7, pp. 1399–1425.

Prelević, D. and Foley, S.F., Accretion of arc-oceanic lithospheric mantle in the Mediterranean: evidence from extremely high-Mg olivines and Cr-rich spinel inclusions from lamproites, *Earth Planet. Sci. Lett.,* 2007, vol. 256, pp. 120–135.

Rehfeldt, T., Foley, S.F., Jacob, D.E., et al., Contrasting types of metasomatism in dunite, wehrlite and websterite xenoliths from Kimberley, South Africa, *Geochim. Cosmochim. Acta,* 2008, vol. 72, no. 23, pp. 5722–5756.

Ripley, E.M., Brophy, J.G., and Li, C., Copper solubility in a basaltic melt and sulfide liquid/silicate melt partition coefficients of Cu and Fe, *Geochim. Cosmochim. Acta,* 2002, vol. 66, pp. 2791–2800.

Sablukov, S.M., On petrochemical series of kimberlite rocks, *Dokl. Akad. Nauk SSSR,* 1990, vol. 313, no. 4, pp. 935–939.

Sablukov, S.M., Sablukova, L.I., and Shavyrina, M.V., Mantle xenoliths from the Zimnii Bereg kimberlite deposits of rounded diamonds, Arkhangelsk Diamondiferous Province, *Petrology,* 2000, vol. 8, no. 5, pp. 466–494.

Samsonov, A.V., Tretyachenko, V.V., Nosova, A.A., et al., Sutures in the Early Precambrian crust as a factor responsible for localization of diamondiferous kimberlites in the northern East European platform, *Abstracts of 10th International Kimberlite Conference, 2012,* Bangalore, 2012, p. 10IKC35.

Samsonov, A.V., Nosova, A.A., Tretyachenko, V.V., et al., Collisional sutures in the Early Precambrian crust as a factor responsible for localization of diamondiferous kimberlites in the northern East European Platform, *Dokl. Earth Sci.,* 2009, vol. 425, no. 2, pp. 226–230.

Sazonova, L.V., Nosova, A.A., Kargin, A.V., et al., Olivine from the Pionerskaya and V. Grib Kimberlite pipes, Arkhangelsk Diamond Province, Russia: types, composition, and origin, *Petrology,* 2015, vol. 23, pp. 227–258.

Schmädicke, E., Gose, J., WittEickschen, G., and Bratz, H., Olivine from spinel peridotite xenoliths: hydroxyl incorporation and mineral composition, *Am. Mineral.,* 2013, vol. 98, no. 10, pp. 1870–1880.

Scott Smith, B.H., Nowicki, T.E., Russell, J.K., et al., Kimberlite terminology and classification, *Proceedings of 10th International Kimberlite Conference,* Pearson, D.G. et al., Eds., *Geol. Soc. India,* 2013, Vol. 2. doi 10.1007/978-81-322-1173-0_1.10.1007/978-81-322-1173-0_1

Sharp, Z.D., A laser-based microanalytical method for the in situ determination of oxygen isotope ratios in silicates and oxides, *Geochim. Cosmochim. Acta,* 1990, vol. 54, pp. 1353–1357.

Sharygin, I.S., Litasov, K.D., Shatskiy, A., et al., Melting phase relations of the Udachnaya-East group-I kimberlite at 3.0–6.5 GPa: experimental evidence for alkali-carbonatite composition of primary kimberlite melts and implications for mantle plumes, *Gondwana Res.,* 2015, vol. 28, no. 4, pp. 1391–1414.

Shchukina, E.V., Agashev, A.M., Kostrovitskii, S.I., and Pokhilenko, N.P., Metasomatic events in the lithospheric mantle beneath the V. Grib kimberlite pipe (Arkhangelsk diamondiferous province, Russia), *Russ. Geol. Geophys.,* 2015a, no. 12, pp. 2153–2172.

Shchukina, E.V., Agashev, A.M., Golovin, N.N., and Pokhlenko, N.P., Equigranular eclogites from the V. Grib kimberlite pipe: evidence for Paleoproterozoic subduction on the territory of the Arkhangelsk Diamondiferous Province, *Dokl. Earth Sci.,* 2015b, vol. 462, no. 1, pp. 497–501.

Shen, T., Hermann, J., Zhang, L., et al., FTIR spectroscopy of Ti-chondrodite, Ti-clinohumite, and olivine in deeply subducted serpentinites and implications for the deep water cycle, *Contrib. Mineral. Petrol.,* 2014, vol. 167, p. 992.

Skinner, E.M.W., Contrasting group I and group II kimberlite petrology: towards a genetic model for kimberlites, *Proceedings of 4th International Kimberlite Conference, Perth, 1989,* Ross, J. et al., Eds., 1989, pp. 528–544.

Skinner, E.M. and Clement, C.R., Mineralogical classification of Southern African kimberlites, *Proceedings of 2nd International Conference,* Boyd, F.R. and Meyer, H.O.A., Eds., Washington, DC: D.C. AGU, 1979, pp. 129–139.

Smart, K.A., Heaman, L.M., Chacko, T., et al., The origin of high-MgO diamond eclogites from the Jericho kimberlite, Canada, *Earth Planet. Sci. Lett.,* 2009, vol. 284, pp. 527–537.

Smith, C.B., Gurney, J.J., Skinner, E.M.W., et al., Geochemical character of Southern African kimberlites: a new approach based on isotopic constraints, *Trans. Geol. Soc. S. Afr.,* 1985, vol. 88, pp. 267–280.

Sobolev, N.V., Logvinova, A.M., Zedgenizov, D.A., et al., Petrogenetic significance of minor elements in olivines from diamonds and peridotite xenoliths from kimberlites of Yakutia, *Lithos,* 2009, vol. 112S, pp. 701–713.

Sobolev, N.V., Sobolev, A.V., Tomilenko, A.A., et al., Paragenesis and complex zoning of olivine macrocrysts from unaltered kimberlite of the Udachnaya-East pipe (Yakutia): relationship with the kimberlite formation conditions and evolution, *Russ. Geol. Geophys.,* 2015, nos. 1–2, pp. 260–279.

Sun, S.S. and McDonough, W.F., Chemical and isotopic systematics of oceanic basalts; implications for mantle composition and processes, *Magmatism in the Ocean Basins,* Saunders, A.D. and Norry, M.J., Eds., *Geol. Soc. London,* 1989, vol. 42, pp. 313–345.

Sweeney, R.J., Prozesky, V., and Przybylowicz, W., Selected trace and minor element partitioning between peridotite minerals and carbonatite melts at 18–46 kb pressure, *Geochim. Cosmochim. Acta,* 1995, vol. 59, pp. 3671–3683.

Taylor, H.O., Jr., Water/rock interactions and origin of H_2O in granitic batholiths, *J. Geol. Soc. London,* 1978, vol. 133, pp. 509–558.

Taylor, H.P., Jr., Frechen, J., and Degens, E.T., Oxygen and carbon isotope studies of carbonatites from the Laacher See district, West Germany and the Alnö district, Sweden, *Geochim. Cosmochim. Acta,* 1967, vol. 31, pp. 407–430.

Tuff, J. and O'Neill, H.St.C., The effect of sulfur on the partitioning of Ni and other first-row transition elements between olivine and silicate melt, *Geochim. Cosmochim. Acta,* 2010, vol. 74, pp. 6180–6205.

Tursack, E. and Liang, Y., A comparative study of melt–rock reactions in the mantle: laboratory dissolution experiments and geological field observations, *Contrib. Mineral. Petrol.,* 2012, vol. 163, pp. 861–876.

Valley, J.W., Kitchen, N., Kohn, M.J., et al., UWG-2, a garnet standard for oxygen isotope ratios: strategies for high precision and accuracy with laser heating, *Geochim. Cosmochim. Acta,* 1995, vol. 59, pp. 5223–5231.

Veksler, I.V., Petibon, C., Jenner, G.A., et al., Trace element partitioning in immiscible silicate–carbonate liquid systems: an initial experimental study using a centrifuge autoclave, *J. Petrol.,* 1998, vol. 39, pp. 2095–2104.

Verichev, E.M., Garanin, V.K., Garanin, K.V., et al., Geology, composition, formation, and prospecting technique of the V. Grib kimberlite pipe, in *Problemy prognozirovaniya, poiskov i izucheniya mestorozhdenii poleznykh iskopaemykh na poroge XXI veka* (Problems of Forecasting, Search, and Study of Mineral Resources on the turn of 21th Century), *Voronezh*: Voronezh. Gos. Univ., 2003, pp. 43–48.

Woolley, A.R. and Kempe, D.R.C., Carbonatites: nomenclature, average chemical compositions, and element distribution, in *Carbonatites: Genesis and Evolution,* Bell, K., Ed., London: Unwin Hyman, 1989, pp. 1–14.

Yaxley, G.M. and Green, D.H., Reactions between eclogite and peridotite: mantle refertilisation by subduction of oceanic crust, *Schweizerische Mineralogische und Petrographische Mitteilungen,* 1998, vol. 78, pp. 243–255.

Zanetti, A., Tiepolo, M., Oberti, R., and Vannucci, R., Trace-element partitioning in olivine: modelling of a complete data set from a synthetic hydrous basanite melt, *Lithos,* 2004, vol. 75, pp. 39–54.

Zhang, H.-F., Mattey, D.P., Grassineau, N., et al., Recent fluid processes in the Kaapvaal Craton, South Africa: coupled oxygen isotope and trace element disequilibrium in polymict peridotites, *Earth Planet. Sci. Lett.,* 2000, vol. 176, pp. 57–72.

Translated by E. Kurdyukov